



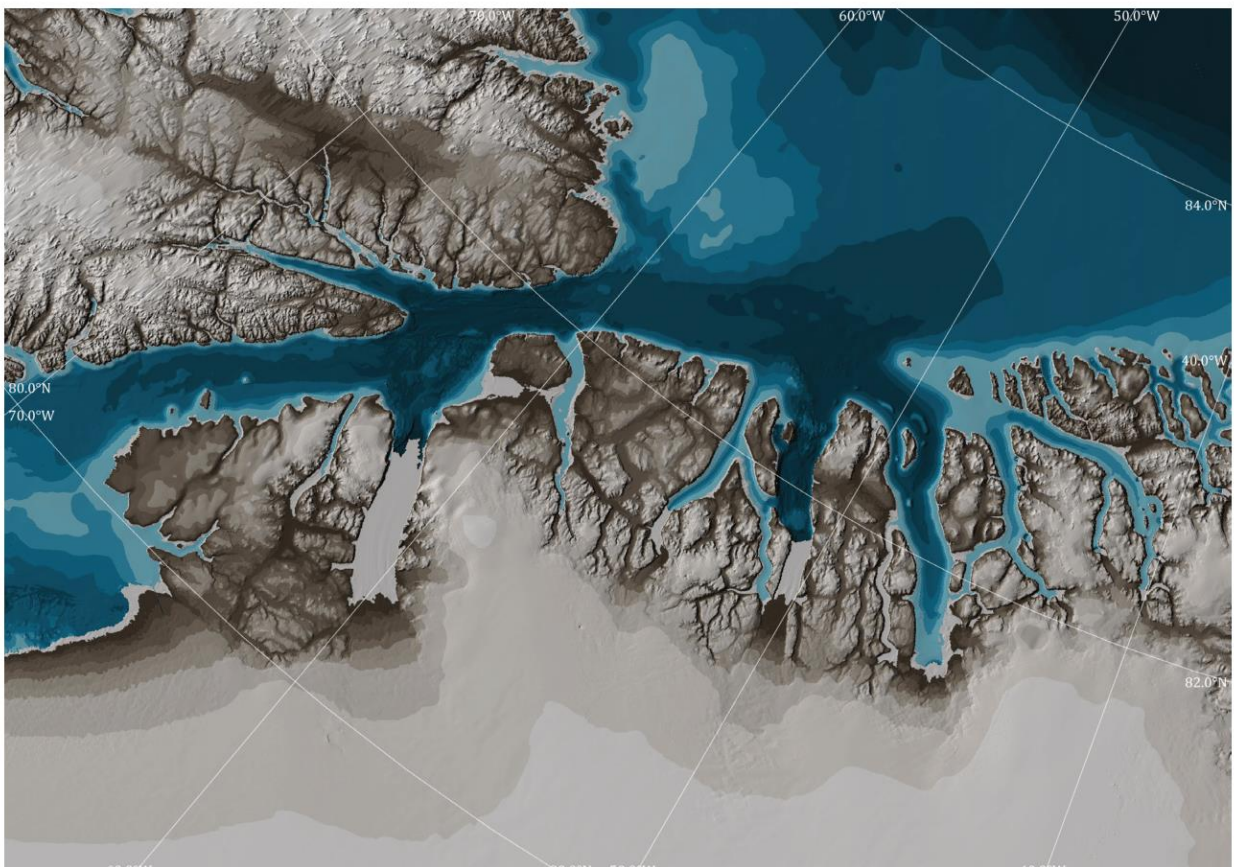
Stockholm
University

Bachelor Thesis

Degree Project
in Marine Geology 15 hp

Influence of seafloor morphology on the retreat of Northern Greenland outlet glaciers under climate warming

Alva Åkerlind



Stockholm 2025

Department of Geological Sciences
Stockholm University
SE-106 91 Stockholm
Sweden

ABSTRACT

In our warming climate, driven by human activity and greenhouse gas emissions, the Greenland ice sheet is shrinking in extent. One of the ways in which the Greenland ice sheet loses mass is through its interaction with warm water at its outlet glaciers. The three adjacent fjords: Petermann fjord, Sherard Osborn fjord, and Victoria fjord, are marine terminating glacial fjords, where the Greenland ice sheet meets the ocean. Comparing the three adjacent fjords, there is noticeable difference in how much of their respective floating ice tongues remain. One of the factors behind this variation is the differences in seafloor geomorphology of the fjords, which controls the inflow of warm water into the fjords. The aim of this study is the comparison of seafloor geomorphology within the fjords in relation to their respective ice masses. Bathymetric data acquired by multibeam echo-sounding from multiple Greenland expeditions were used for the morphological mapping done in QGIS. The study results show varied seafloor landforms throughout the three fjords, with more sedimentary landforms such as grounding-zone wedges and moraines present in the Petermann and Sherard Osborn fjords, and Victoria fjord instead dominated by rough bedrock structures. A possible interpretation of the results is that the presence of sedimentary landforms formed at longer standstills during past ice retreat episodes act as barriers against warm water inflow, keeping the floating ice tongues from collapsing. In our continuously warming climate, deepening the knowledge on ice-ocean interaction and ice sheet melting is of critical importance. This study aims to contribute some new insights to that area.

Keywords

Bathymetry; ice sheet melt; glacial submarine landforms; geomorphology; fjord; outlet glacier; marine geophysical mapping.

Table of contents

List of figures and tables	4
Abbreviations	5
1 Introduction	6
2 Background	7
2.1 Geological setting	7
2.1.1 Arctic physical oceanography	7
2.1.2 Arctic seafloor geomorphology	9
2.1.3 Northern Greenland glacial fjords	10
3 Method	13
3.1 Previous data acquisition	13
3.2 Mapping and data analysis	14
4 Results and Interpretation	15
4.1 Petermann fjord	15
4.2 Sherard Osborn fjord	18
4.3 Victoria fjord	21
4.4 Bathymetric profiles	24
5 Discussion	26
5.1 Observed landforms	26
5.2 Controls on ice tongue melting	26
5.3 Study limitations	28
5.4 Broader implications and future research	28
6 Conclusions	29
7 Acknowledgements	30
8 References	31
8.1 Literature	31
8.2 Data sources	33
Appendix A	34

List of figures and tables

Figure 1. Arctic Ocean overview map	7
Figure 2. Fram Strait	8
Figure 3. Nares Strait	9
Figure 4. Arctic Ocean water circulation	9
Figure 5. Greenland ice sheet flow velocity	10
Figure 6. Northern Greenland fjord locations	11
Figure 7. Multibeam echo-sounding	13
Figure 8. Petermann fjord bathymetry	15
Figure 9. Petermann fjord seafloor landforms	17
Figure 10. Petermann fjord aspect	18
Figure 11. Sherard Osborn fjord bathymetry	19
Figure 12. Sherard Osborn seafloor landforms	20
Figure 13. Sherard Osborn aspect	21
Figure 14. Victoria fjord bathymetry	22
Figure 15. Victoria fjord seafloor landforms	23
Figure 16. Victoria fjord aspect	24
Figure 17. Bathymetric profile lines	24
Table 1. Large-scale geomorphic features of the Arctic Ocean	9
Table 2. Small-scale features of Petermann fjord	17
Table 3. Small-scale features of Sherard Osborn fjord	20
Table 4. Small-scale features of Victoria fjord	23

Abbreviations

AO	Arctic Ocean
BS	Bathymetric sill
FS	Fram Strait
GIS	Geographical information system
GrIS	Greenland ice sheet
GZW	Grounding-zone wedge
IB	Icebreaker
IBCAO	International bathymetric chart of the Arctic Ocean
LGM	Last glacial maximum
MBES	Multibeam echo-sounder
MBSL	Meters below sea level
MSGL	Mega-scale glacial lineation
NA	North Atlantic
NS	Nares Strait
OFG	CH Ostenfeld glacier
PF	Petermann fjord
PG	Petermann glacier
RG	Ryder glacier
RV	Research vessel
SOF	Sherard Osborn fjord
TWT	Two-way travel time
VF	Victoria fjord

1 Introduction

Oceans cover the majority of Earth's surface. Some of our surface-layer oceans are perennially or seasonally frozen as sea ice. Sea ice is present around Antarctica and in the Northern polar region (Figure 1) and where some parts remain frozen for years on end (Skinner & Murck 2011). In our current interglacial climate, ice sheets cover around 10% of the surface (Marshall 2005; Skinner & Murck 2011). This area, together with the perennially frozen ground and the sea ice, constitutes the cryosphere (Skinner & Murck 2011). The ocean and the cryosphere are in constant and continuous interaction with each other and together make up a significant part of Earth's climate system ().

The high albedo of the glaciers and sea ice have a cooling effect on the climate, by reflecting much of the Sun's incoming radiation instead of letting it be absorbed and turned into heat by the Earth. The reduction in ice and snow cover on Earth's surface lowers its albedo. Especially as what was formerly covered by bright-colored snow and ice instead becomes areas of dark boreal forests and sea water, both of which absorb much radiation (Ruddiman 2014). With global climate change primarily driven by an increase in atmospheric greenhouse gas concentrations, from anthropogenic emissions, the ice and snow coverage is decreasing. The sea-ice decrease and glacial snow melt that usually takes place in summer is intensifying and leading to a longer season of ice melting as well as greater melting intensity (Elmes *et al.* 2021). The melting of the Greenland ice sheet would lead, not only to a decrease in the planetary surface albedo, but also to rise of the global mean sea level. Within the ice sheet of Greenland, water equivalent to a 7.42 m rise in global sea levels is captured (Morlighem *et al.* 2017).

The melting of marine terminating glaciers is in large due to the ice-ocean interaction

and transportation of warm ocean water, which melts the ice it encounters (Jakobsson *et al.* 2018; Mashayek 2023). The large-scale global ocean circulation is mainly steered by the major submarine landforms of tectonic origin, such as continental shelves, continental slopes and mid-ocean ridges. Smaller landforms do, however, also play a role in influencing circulation on a smaller scale, which may affect processes such as glacial melt significantly (Mashayek 2023).

The three adjacent outlet glaciers in the fjords of northwestern Greenland: Petermann fjord, Sherard Osborn fjord, and Victoria fjord, are all at different stages regarding ice tongue melting. Petermann has a large part of its ice tongue remaining, despite large calving events in 2010, while the Sherard Osborn fjord sees less floating ice (Jakobsson *et al.* 2020b), and the Victoria fjord almost none.

The aim of this study is to classify and quantify submarine glacial landforms in the three abovementioned fjords, to make comparisons between different landform assemblages in relation to ocean water circulation and in turn the glacial ice melt of marine terminating glacial outlets. The study focuses on ice-ocean dynamics and examines past melting events in relation to the individual fjords' seafloor topography. The following questions were formulated to enclose the study aim:

1. What different submarine landforms and landform assemblages can be observed in the three adjacent fjords?
2. Are there observed differences in the fjords' bottom topographies that explain variations in ice-tongue melting and stability among the three outlet glaciers?

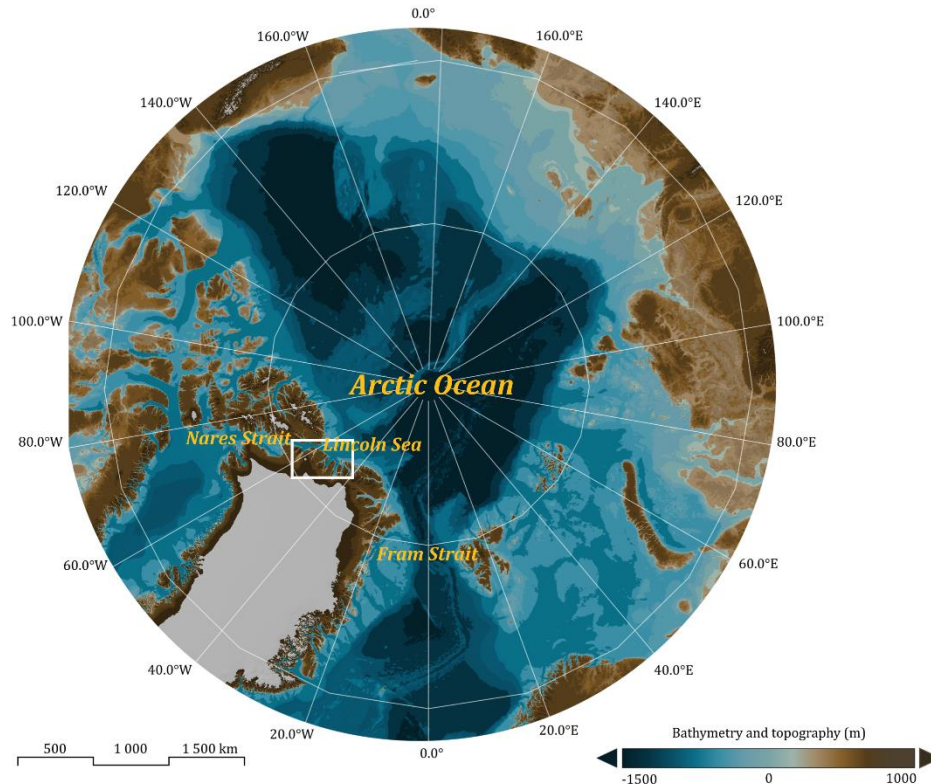


FIGURE 1 Overview map of the Arctic Ocean with longitudinal coordinates. The coloring corresponds to bathymetry and topography for blue and brown values respectively. The Greenland ice sheet is visible in white coloring. The white rectangle shows the study area. The bathymetric data is from the International Bathymetric Chart of the Arctic Ocean (IBCAO) version 5.0 (Jakobsson *et al.* 2024).

2 Background

This study focuses on bathymetric multibeam echo-sounder (MBES) datasets acquired during three separate research expeditions with icebreaker (IB) Oden to the Arctic Ocean (AO) and northern Greenland. MBES data was acquired onboard IB Oden and research vessel (RV) Skidbladner. Bathymetry refers to the depth of the seafloor, much like the topography of land (Weatherall *et al.* 2015). The first expedition focused on the Petermann glacial fjord, took place in 2015 (Mix *et al.* 2015). The second expedition, in 2019, targeted the Sherard Osborn fjord, where the Ryder Glacier drains (Jakobsson *et al.* 2021). The third expedition, in 2024, explored Victoria fjord where CH Ostenfeld glacier drains (The GEOEO Shipboard Scientific Party, 2025).

The severe presence of sea ice in the Lincoln Sea makes northern Greenland a difficult location for conducting research, hence

much of its geology and glaciology remains unknown and poorly understood.

2.1 Geological setting

Greenland is a large island of the northern hemisphere, covered by a thick continental ice sheet (Figure 1). The island is situated between the AO in the North and the North Atlantic Ocean (NA) in the South. Located between eastern Greenland and Svalbard is the Fram Strait (FS), the largest passage for water between the two oceans. FS is also where the Arctic deep water is formed and transported southwards through the NA (de Steur n.d.).

2.1.1 Arctic physical oceanography

The AO is a small part of the world ocean, which in total covers more than 70% of Earth's surface (NOAA 2024). It is closely

connected with the NA and the North Pacific Ocean. According to the definition by the International Hydrographic Organization (IHO), the boundary between the Arctic and NA is lies along the southwestern coast of Norway. It continues westwards along the southern coast of Greenland, to the coast of Labrador, Canada. The AO sees its boundary to the Pacific along the coast of the Alaskan Sward Peninsula and westwards to the coast of the Russian Chukotovski peninsula (IHO 2002).

The AO is also the northernmost and smallest of the five named oceans (NOAA n.d.). It is especially landbound and semi-enclosed. Compared to the other oceans, the AO has a particularly dramatic and variable history, with alternating glacial and interglacial periods. With the different past extents of ice coverage in the Arctic and the periodic retreats of the ice, the AO seafloor hosts a great variation of submarine landforms. Many, if not most, have been shaped by the movement, formation, melting, and retreat of glacial ice during past glaciations and deglaciations (Jakobsson *et al.* 2014).

The Arctic region is especially susceptible to climate change, which is already noticeable in the clear decrease of annual sea ice. Since 1979, the Arctic has warmed almost four times more than the global average (Rantanen *et al.* 2022). During winter, the entirety of the AO is covered in sea ice, most of which melts away during the following summer. The amount that remains frozen for several consecutive years is rapidly declining as more and more sea ice melts away in the summer (Timmermans & Marshall 2020).

The presence of sea ice in the AO greatly affects regional and global ocean circulation, both in the surface water and deeper down in the water column. The amount of sea ice present affects the wind forcing on the ocean surface, which is the main driver of sea-surface circulation (Timmermans & Marshall 2020). With formation and melting of sea ice, the salinity is altered as well. During the melting of sea ice in the summer,

the surface water decreases in salinity. The winter formation of sea ice instead results in brine rejection, the leaving-behind of salt content from the ocean water as it forms fresher-than-water ice (Talley *et al.* 2011).

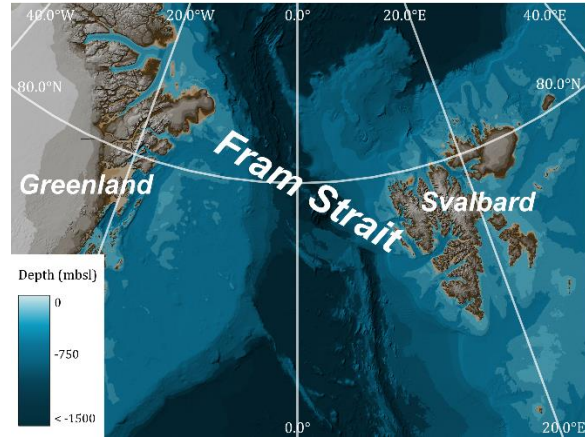


FIGURE 2 Map displaying the FS and its approximate orientation, located between northeastern Greenland and western Svalbard.

Besides the locally formed deep and bottom waters, much of the water circulating in the AO basins enters via the NA current traveling on the eastward side of the NAO, along the western coast of Norway. Atlantic water (AW) enters central AO at two locations, through the Fram Strait (FS) and across the Barents Sea. The FS branch is intermediate in depth, ca 100 - 900 m, which the Barents Sea branch is shallower, 50 - 300 m. The AW eventually goes deeper to circulate around central AO. Deep water flows out through the FS, below the AW (Figure 2). NA water is significantly warmer than both above and below laying water masses in the central AO, thus heating up the AO and melting the sea ice it meets (Rudels *et al.* 2012; Timmermans & Marshall 2020).

After having entered through the FS, the AW generally circulates through the AO cyclonically, continuing to the Canadian Basin. The area around northwestern Greenland and Ellesmere Island features some of the thickest sea ice in the AO, making the flow of AW in the region especially important for global climate future and sea ice loss. The Nares Strait (NS) (Figure 3), between the west of Greenland and Ellesmere Island, connects Baffin Bay in the south with the rest of the AO in the north,

making it an important passage for circulation (Münchow *et al.* 2011).

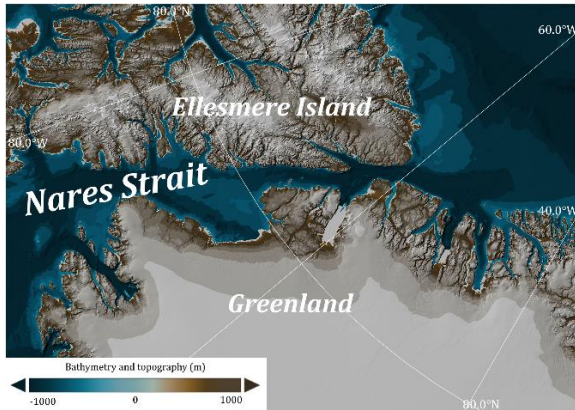


FIGURE 3 Nares Strait and its placement between Ellesmere Island and Greenland. To the center-right of the map, the three examined fjords (Petermann, Sherard Osborn and Victoria fjords) are visible.

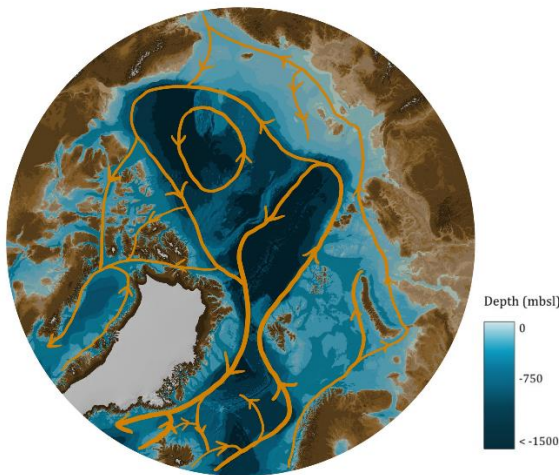


FIGURE 4 General circulation patterns of the AO. Based on a combination of data from Talley *et al.* (2011) and Cook (*n.d.*).

2.1.2 Arctic seafloor geomorphology

The seafloor can be categorized differently based on spatial scale. Largest, and most generalized, is the division into 1) continental shelf, 2) continental slope, 3) abyssal plain, and 4) hadal zone. These four categories are mutually exclusive, with clear definitions for each. Nearest to land is the continental shelf, followed by the slope, and finally the abyssal plains. Hadal zones are defined as the areas of sea depths >6000 m (Harris *et al.* 2014). Since the AO is generally

not deeper than 4000 m deep, with its deepest location the Molloy Deep reaching 5669 m (Stewart & Jamieson 2019), no Hadal zones are present (Timmermans & Marshall 2020).

Some prominent intermediate and small-scale seafloor landforms of the AO are glacial troughs, which are found over a larger area in the Arctic than any other ocean, (besides Southern Ocean) (Harris *et al.* 2014). Additionally, canyons, abyssal plains and hills, rises, plateaus, terraces, shelves, and a ridge are widespread features in the AO. For example, the Lomonosov ridge is a ridge of continental crust, separating the two main AO basins (Cochran *et al.* 2006; Harris *et al.* 2014).

Here, large-scale refers to features of basin scale, while small-scale is used for smaller features superimposed on the larger ones.

TABLE 1 Large-scale seafloor features in the AO in percentage of basin area, compared to global averages. These are all features of which the highest percentage of basin area covered are in the AO. Reworked with data from Harris *et al.* 2014.

Seafloor feature	Arctic Ocean (%)	Global average (%)
Continental shelf	51.8	8.91
Plateau	9.19	5.11
Spreading ridge	4.76	2.19
Shelf valley	14.0	1.31
Canyon	16.1	11.2
Terrace	24.6	11.6

By areal percentage, the AO is the ocean region with the largest proportion of continental shelf (Table 1). Continental shelf is defined as “the flat or gently sloping region adjacent to a continent or around an island that extends from the low line to a depth, generally about 200 m, where there is a marked increase in downwards slope.” (SCUFN *n.d.*). Other relatively large features are spreading ridges, an elongated feature found at diversion zones; shelf valleys, elongated depressions of the seafloor along the continental shelf edge with depths exceeding 10 m and length exceeding 10 km (Harris *et al.* 2014); as well as terraces, which are relatively flat areas with slopes on

either side, one side descending and the other ascending. The ascending slope is steeper than the descending slope (SCUFN n.d.). Seafloor features that are completely absent in the AO include hadal zones, guyots, trenches, and coral reefs (Harris *et al.* 2014).

Most of the intermediate and small-scale landforms of the AO seafloor are of glacial origin. During glaciated periods, the presence of glacial ice will reshape the land below, in front of, and around it. The glacial landforms created can be classified as either 1) subglacial, formed underneath the ice sheet; 2) ice-marginal, which are formed at the ice margin during periods of retreats and advances of the ice sheet; and 3) glaciomarine, which are the byproduct of glacial calving at the ice-ocean termination site (Jakobsson *et al.* 2014; Batchelor *et al.* 2023). Subglacial landforms are generally streamlined in the direction of ice flow, while ice-marginal landforms are oriented in the direction of the ice face, perpendicular to the ice flow. Glaciomarine landforms are more irregular in their morphology (Batchelor *et al.* 2018). Some examples of subglacial landforms are mega-scale glacial lineations (MSGs), elongate ridges aligned in the flow of the ice direction, and crag-and-tails, which are also streamlined, but occur at sites of bedrock obstacles, with a rough bedrock side and an along-flow “tail” of sediments in the direction of the ice flow. Ice-marginal landforms can be elongate ridges, perpendicular to the ice flow direction, as in the case of moraines, or larger rounded sediment deposits formed at longer standstills during the ice retreat: grounding-zone wedges (GZWs). Glaciomarine landforms include iceberg ploughmarks, which are erosive scours left on the seafloor from the abrasion of drifting icebergs against the floor.

2.1.3 Northern Greenland glacial fjords

Greenland has the largest glacial ice sheet on Earth besides Antarctica, with the current climate. The Greenland ice sheet (GrIS) is experiencing visible mass loss on a decadal scale, both from steady long-scale decrease in ice mass, as well as from catastrophic melt

events (Elmes *et al.* 2021). The shape of the GrIS has a topography characterized by elevation of the ice in the middle section of the island where most of the precipitation is deposited, around which the ice sheet slopes down towards the coast. The highest points of the Greenland surface may reach 3200 m above sea level (NASA n.d.).

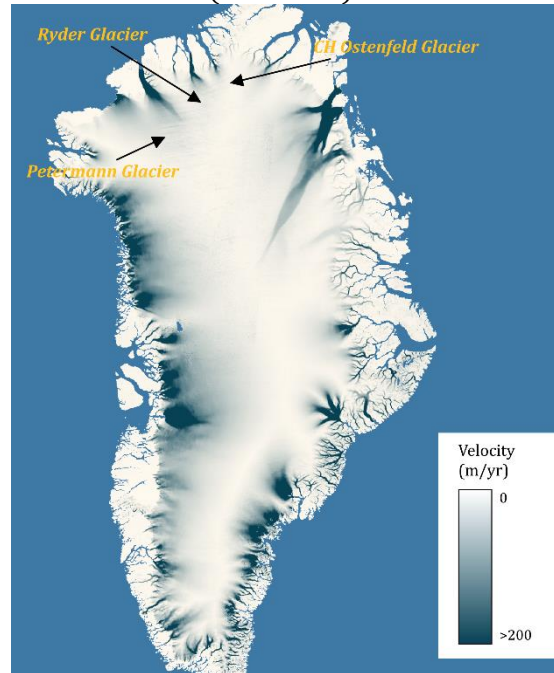


FIGURE 5 The variation in ice flow velocity of the Greenland ice sheet. Darker corresponds to higher velocities. The northernmost ice streams visible are those of Petermann glacier, Ryder glacier, and C.H. Ostenfeld glacier. Data from ESA Climate Change Initiative Greenland.

The flow direction of the ice is downwards through the ice column as well as towards the coastal area, where the island and ocean are bound together by fjords. Within the larger flow dynamics, there are some prominent larger ice streams draining the GrIS at a substantial rate (Figure 5). Ice streams are parts of the ice sheet where the ice flow velocity is significantly greater than the surrounding areas. Ice streams are generally not exclusively controlled by topography, unlike outlet glaciers (Bennett 2002). The northern ice streams of GrIS flow out into the outlet glaciers of the Petermann fjord, Sherard Osborn fjord and Victoria fjord respectively. Outlet glaciers are present in the fjords as either ice cliffs, bound to the bed of the fjord, or floating in the shape of ice tongues. The ice tongues stabilize the outlet glaciers by exerting so

called buttressing forces. When the ice tongues break up through massive calving,

the outlet glaciers may be destabilized. (Jakobsson *et al.* 2020b).

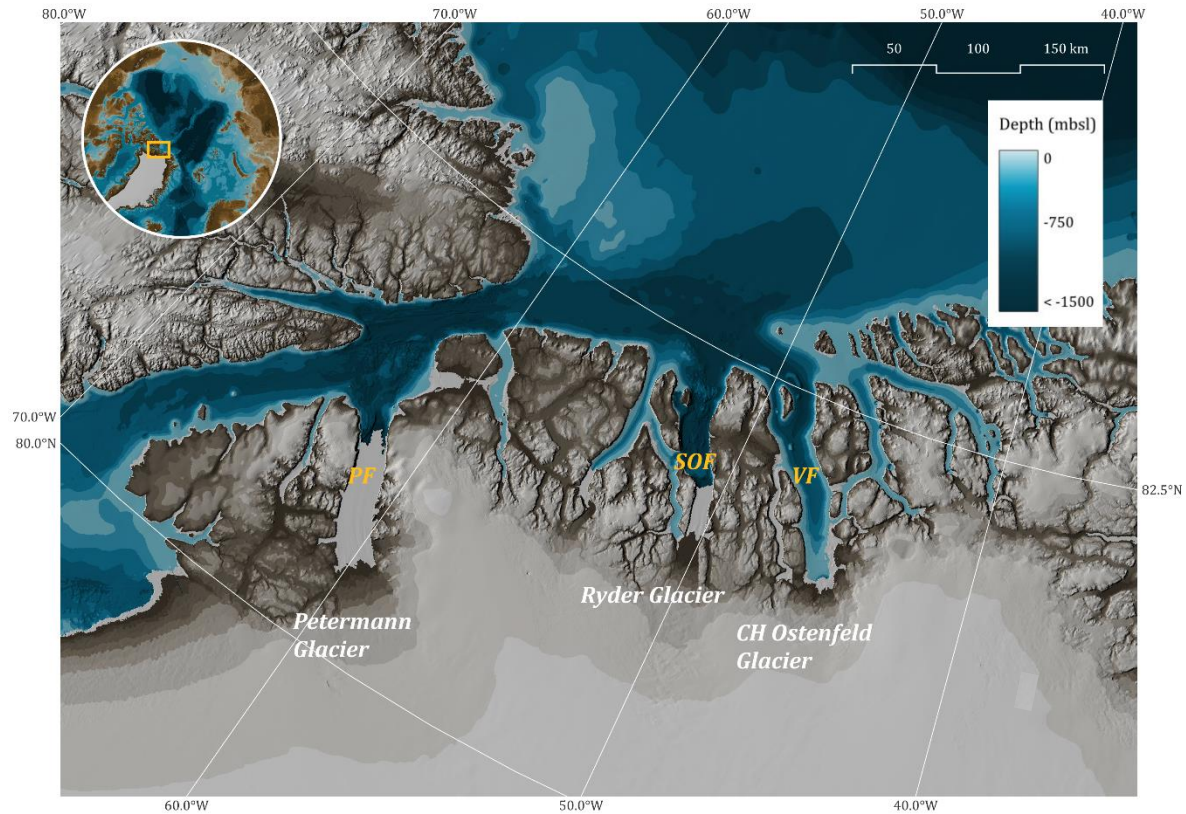


FIGURE 6 Proximity of the three studied fjords in Northwestern Greenland and their adjacent glaciers. Petermann glacier and Petermann fjord; Ryder glacier and Sherard Osborn fjord; and C.H. Ostenfeld glacier and Victoria fjord. The inset shows the location of the studied area within the Arctic Ocean.

2.1.3.1 Petermann fjord

The Petermann fjord (PF) is the westernmost of the three adjacent marine terminating glacier fjords of northwestern Greenland examined in this study, draining the Petermann glacier (PG) (Figure 6).

PF reaches depths of over 1100 m and has a pronounced bathymetric sill (BS) at the entrance to the fjord, with depths generally less than 400 mbsl. A BS is a raised section of the seafloor which separates deeper water basins by acting as a barrier that restricts water exchange. Both the fjord and the NS area have landforms typically formed by a glacial past. Previous studies have identified MSGs and other streamlined features such as drumlins and crag-and-tails in the fjord following the direction of the fjord, as well as in the NS in a northeastern direction. The BS has been interpreted as a GZW (Jakobsson *et al.* 2018; Hogan *et al.* 2020).

The fjord encountered major calving events of its ice tongue during 2001, 2008, 2010, and 2012. Especially devastating ice loss was seen in 2010 and 2012 (Münchow *et al.* 2016). The main driver of its ice volume loss since the first available data from the 1800s seems to be driven by the ice-ocean interaction underneath the ice tongue rather than calving at the front (Johnson *et al.* 2011). The fjord sees fast flow rates of the ice and loses most of its mass through melting of the ice tongue from warm water interacting with the floating ice tongue from below. In 2018, the ice tongue of PF was estimated to be 43 km in length and 20 km in width. Close to 40% of the ice tongue extent was lost in the two major calving events in 2010 and 2012 (Münchow *et al.* 2016).

The renewal of NA water from the NS into the fjord appears to occur relatively

frequently by passing over the fjord sill, which reaches a maximum depth of 443 mbsl (Jakobsson *et al.* 2018). The input of NA water has led to a long-term retreat of the ice tongue, besides the major calving events, of 311 m/yr in average between the years 1948 and 2015 (Jakobsson *et al.* 2020b).

2.1.3.2 Sherard Osborn fjord

The Ryder glacier (RG) meets the ocean through the Sherard Osborn fjord (SOF), an approximately 55 km long fjord (Figure 6), counted from the middle of its outer sill to its ice-tongue, with a maximum width of 17 km (Jakobsson *et al.* 2020a). SOF drains the RG into the Lincon Sea, adjacent to the northern part of Greenland. The RG drains around 1.4% of the GrIS (Hill *et al.* 2017). The Ryder ice tongue is approximately 55 km in length, from the innermost floating part to the outer front. Between the years 1948 and 2015 the ice tongue of SOF saw an advance of 43 m/yr in average (Hill *et al.* 2018). During the whole of the Holocene, the Ryder ice tongue has overall retreated, in line with the deglaciation after the LGM. The current ice tongue likely remains due to the stabilizing effect offered by the seafloor features of the SOF, preventing some of the inflow of warm NA water (Jakobsson *et al.* 2020b; O'Regan *et al.* 2021).

The SOF contains two BSs. The inner BS is interpreted to be a GZW as its surface is flat and made up of glacial sediments. The outer

BS is instead interpreted as bedrock structures. Unlike SOF, PF only has one BS, a possible explanation for the difference in past behaviors between the glaciers' respective ice tongues. Comparison with previous observations in the early 1900s shows that the RG ice tongue, like the Petermann ice tongue, has seen a long-term retreat due to climate warming (Jakobsson *et al.* 2020b; O'Regan *et al.* 2021).

2.1.3.3 Victoria fjord

The CH Ostenfeld glacier (OFG) drains into the Victoria fjord (VF) (Figure 6). VF has nearly no ice tongue remaining since large melting events took place between the years 2000 and 2006 (O'Regan *et al.* 2021). The current OFG ice tongue is around 8 km wide and 1.5 km long from the southernmost floating point to its terminus. Previous observations and aerial photography describe a 25 km long ice tongue within the VF during the latter half of the 20th century. This would mean a 94% decrease in ice tongue extent during the past 50 years or so (Furlotti 2024).

Because of the remote location and difficult-to-reach conditions, no data have been published on the bathymetry and seafloor conditions of the VF. The recent MBES data acquired from the IB Oden expedition to north Greenland in 2024 are the first ever available from VF and yet to be integrated into the IBCAO dataset.

3 Method

The methodology consists of two main stages: data acquisition and processing, followed by data analysis.

3.1 Previous data acquisition

A MBES maps the seafloor bathymetry in a two-dimensional manner as illustrated in Figure 7. Some insight into the geology of the seafloor is also provided by the MBES backscatter. Soft sediments generally reflect less of the sound compared to hard bedrock. Unlike earlier single-beam echo sounding techniques that only provide bathymetric data for a one-dimensional line right below the instrument, MBES gives two-dimensional spatial information due to its wide swath width. MBES uses transmitters mounted to the hull of the vessel to transmit a sound pulse of a decided frequency. The acoustic pulse reflects off the seafloor and returns to the vessel where it is read by a receiver. The two-way travel time (TWT), the time taken for the acoustic signal to reach seafloor and return to the receiver, is calculated (NOAA 2009; Jakobsson *et al.* 2016). Half of the TWT is used together with known values for sound velocity (v) in water to calculate the depth (D) according to:

$$D = v \times \frac{TWT}{2} \quad (1)$$

The horizontal resolution of the MBES is dependent on its sampling frequency, the beam width, and the wave phase at the bottom of the pulse. The frequency used and the length of the transducer array also has great impacts on the achieved horizontal resolution (Jakobsson *et al.* 2016).

An MBES system uses a set angle of which it transmits the acoustic pulses, but the width it corresponds to is related to the water depth. The deeper it is, the wider the swath width will become. Common for modern MBES is a swath angle in the range of 130° - 150° in the across-track direction. The along-track direction is instead made narrow, around 0.5° - 5° for modern MBES,

to decrease the seafloor footprint of the pulse. The result is a thin fan-shaped area studied at each acoustic signal from the MBES (Jakobsson *et al.* 2016).

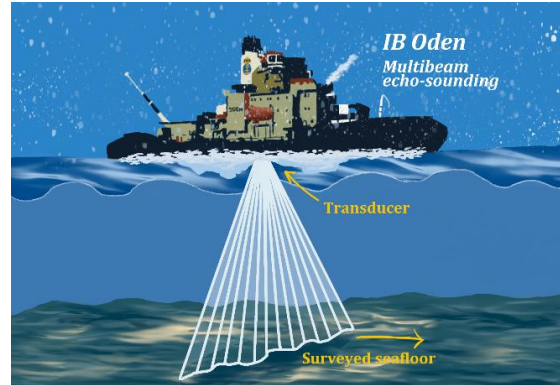


Figure 7 Schematic of IB Oden and its MBES fan-shaped survey area. Reworked from an image by I Jakobsson (2018).

The bathymetric data used in the study was acquired onboard IB Oden using a hull-mounted Kongsberg EM122 $1^\circ \times 1^\circ$, 12 kHz MBES. This model of MBES can operate at depths from 20 to 11 000 m, well suited for the depth range of approximately 200 to 1200 m found in the studied area. Its swath angle is 150° and may result in a swath width of up to 6 times the water depth in the deepest waters. It uses 288 beams and up to 846 soundings per emitted ping (Kongsberg 2006).

RV Skidbladner is a smaller vessel, 6.4 m in length, with a bow-mounted MBES in the 200 - 400 kHz range, able to reach around 500 mbsl. Most of the geophysical mapping was done using IB Oden, with RV Skidbladner instead used at sites near shore (Jakobsson *et al.* 2020a).

Most of the studied data is openly available for download via the Bolin Centre Database. At the point of downloading, the data had already been inspected and processed with regards to data quality, been run through algorithms to choose best-suited grid resolution amongst other things and projected using the IBCAO-version Polar Stereographic coordinate system. Much of the data processing was done onboard IB

Oden during the expedition in the ship's laboratory environment (Jakobsson *et al.* 2020a). The IBCAO v.4 dataset uses a 200 x 200 m grid-cell, with much of its bathymetric data acquired by MBES (Jakobsson *et al.* 2020c).

3.2 Mapping and data analysis

The bathymetric data was analyzed visually and mapped in QGIS version 3.38. All three fjords were mapped using the same format and mostly the same settings. A hillshaded layer of the respective fjord bathymetry with a Z-factor of 3.00 was made the foundation. The Z-factor was set to 3.00 after some testing as it displayed slopes and heights well without overexaggerating to the point of being misleading. The hillshade altitude was set to 45.00° for all three fjords and the azimuth at 315.00° for PF and SOF, and 3.00° for VF. There is a difference in resolution between the datasets, with the PF and SOF datasets as processed grids at resolutions of 15 x 15 m and the VF dataset at 30 x 30 m. Resolution differences, as well as the observed differences in seafloor morphologies made the different settings necessary for the hillshaded layers.

Above the hillshaded layer, a new layer displaying bathymetry, blended by multiplication, was added with singleband pseudocolors in a green-blue-purple color gradient. The bathymetric band used a linear interpolation with equal interval of 10

classes. This setup allowed for mapping of the seafloor landforms in vector format. Linear forms such as MSGs, crag-and-tails, and moraines were mapped by digitizing line strings along the features. The GZWs and meltwater channels were mapped with polygons, and rough bedrock areas using mapped with polygons.

General directions of the slopes within the three fjords, indicative of past ice flow direction, were examined using Aspect with a color gradient containing four distinct colors, each assigned to the direction of 0°, 90°, 180°, and 270° respectively. The general trends of directional coloring in the Aspect study were combined with individual identified landforms to build an understanding of the general landform assemblages and past glacial behaviors in the area.

Using polylines drawn from the innermost of the fjords, available from the data to the outer parts of the datasets, height profiles were plotted from the three fjords and compared. The profiles were drawn using the data provided by the terrain profile plugin in QGIS (Profile tool, plugin ID: 87), which was then processed and used to draw plots in Python using the Matplotlib and Pandas libraries. The profile lines were not drawn as straight lines, but with an attempt to follow the approximate curvature of the fjords and thus the assumed water circulation path.

4 Results and Interpretation

The bathymetry and seafloor landforms of the three fjords are noticeably different in many ways, but there are many similarities as well. All three sites have landforms of largely glacial origin, with typical glacial seafloor landforms such as GZWs, MSGs, crag-and-tails, meltwater channels, rough bare-scraped exposed bedrock, and clearly defined direction of the landforms, corresponding to past glacial ice flow.

4.1 Petermann fjord

The PF area studied covers around 3200 km² and has depths within the range of approximately 200 mbsl to slightly more than 1100 mbsl. Its deepest parts are present within the fjord area, where depths

are typically around 1000 mbsl (Figure 8). At the entrance to the fjord, there is a BS, identified to be a GZW. This has been interpreted by previous studies to have been formed from continued deposition of glacial sediments and till during a glacial retreat standstill at the grounding line of the ice sheet at or near the last glacial maximum (LGM) (Jakobsson *et al.* 2018). The BS covers an area of just above 100 km², corresponding to 3.1% of the total PF area. Around 9 600 m further out from the fjord, there is another smaller GZW (Figure 9b). The height of the BS compared to surrounding seafloor is 100 m on the northern side, and 300 m on the fjord side. The outer GZW sees a height of between 200 and 400 m relative to its surroundings, depending on which side. Its areal coverage is 68 km², or 2.1% of the total area.

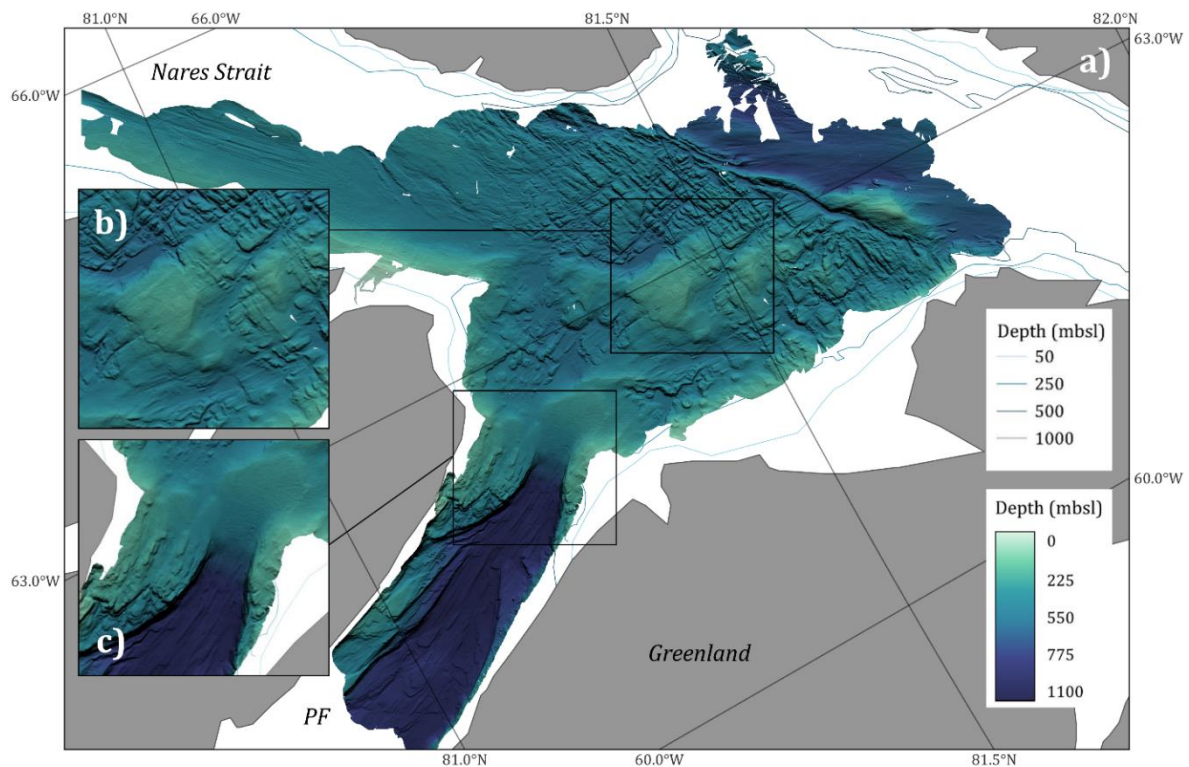


FIGURE 8 (Previous page) *Bathymetry of the Petermann fjord, the outlet glacier where the Petermann glacier drains. a) Darker blue and purple colors correspond to deeper depths, and lighter blue to green colors are shallower areas. The map uses the EPSG:3996 EGS 84 / IBCAO Polar Stereographic projection. The contours in blue shades display water depth outside of the high-resolution area. b) A rough-textured seafloor and the upper GZW. c) The lower GZW acting as a bathymetric sill at the entrance to the fjord.*

The western part of the area in the NS is mainly categorized by flat terrain overlain by MSGs in SW-NE direction and iceberg ploughmarks scattered across the site, and to some degree superimposed on the MSGs (Figure 9). This is the main site for MSGs within the PF area, though additional ones can be found across the whole site and within the fjord especially. All PF MSGs vary in length between 1 km and 21 km, with 4.9 km as median and 5.8 km as mean lengths. Shorter MSGs are found within the fjord, where the range is 3 to 8 km, compared to the range of 3 to 13 km long in the NE region of the PF area. The iceberg ploughmarks are between <1 km and 9 km in length.

The northern part of the area is defined by large meltwater channels in an approximately NNW-SSE direction. The meltwater channels vary in width between 200 and 650 m, with some larger features reaching widths of up to 1000 m and beyond. The area cut through by meltwater channels is defined by rough bedrock terrain, likely covered by at most a very thin layer of sediments.

The seafloor type described as rough bedrock covers a total area of 0.756 km², making rough bedrock around 23.6% of the whole area's seafloor. The rough bedrock terrain is mainly limited to the northern part of the PF area, with some smaller sections between the inner and outer BSs as well as in the fjord. Superimposed on the rough bedrock is not only meltwater channels, but also transverse moraine ridges generally

found in an NNW-SSE direction. The moraine ridges are interpreted as having been formed during shorter stand-still periods of the GrIS at the grounding line site. They may also occasionally be formed from short readvances. The moraines are between 3 km and 36 km in length, with the median and mean both found around 10 – 11 km. The shorter moraines are found within the fjord, and longer ones to the NE of the area. The longest moraine at 36 km runs almost across the entire section of the NS, from Ellesmere Island to Greenland. The area north of this moraine is deeper than the central area and mostly flat with only the presence of MSGs and iceberg ploughmarks.

Crag-and-tails are found in two main areas: within the fjord and in the middle region around the GZWs. They are oriented in the same direction as the MSGs of the fjord, from SW-NE, with slight variations in accordance with the general turning angle of the fjord. The crag-and-tails in the middle part, to the east of the GZWs, are slightly more eastern in their orientation. The variation in lengths of the PF crag-and-tails is between 1 km and 5 km, with shorter lengths of 1-3 km found more frequently.

Small hills have also been identified along the sides of the fjord. These hills are assumed to be bedrock outcrops or possibly boulders or blocks from previous mass movement events at the fjord walls. This landform is not found anywhere else in the PF area.

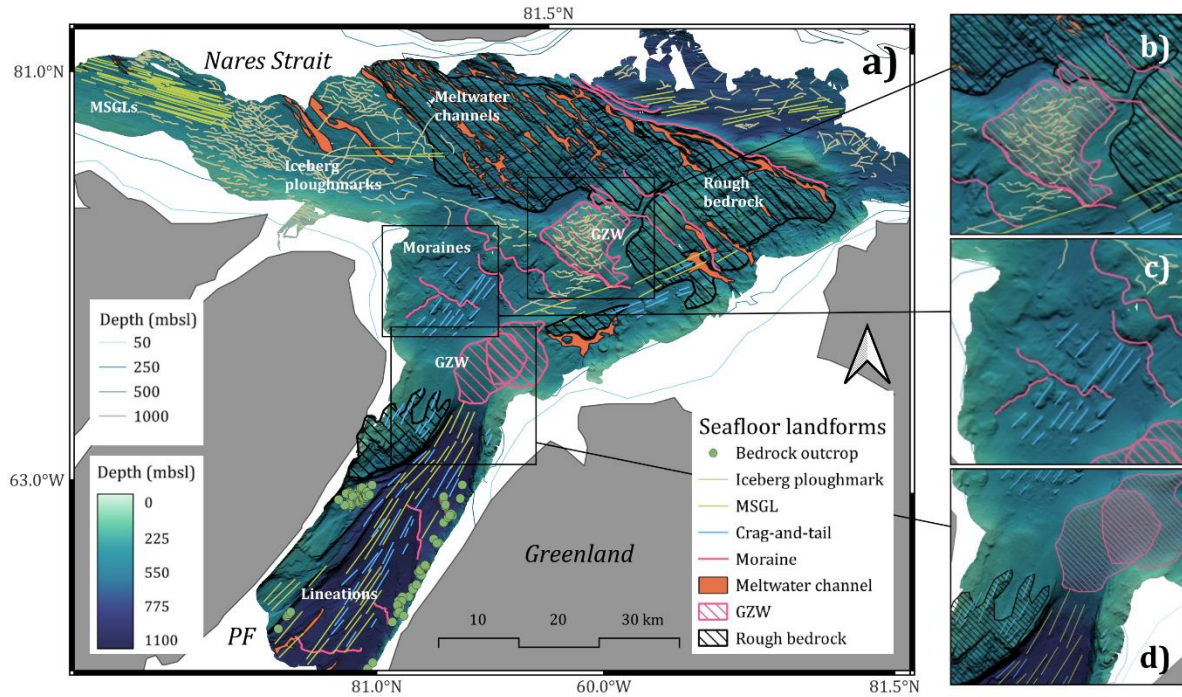


FIGURE 9 Identified seafloor landforms of PF and parts of NS. **a)** Overview of the identified landform assemblages. **b)** The outer GZW, with superimposed iceberg ploughmarks. North of the outer GZW, the area is dominated by rough bedrock terrain. **c)** The middle region is characterized by crag-and-tails and moraine ridges. **d)** The fjord entrance characterized by its GZW acting as a BS and lineations (both MSGLs and crag-and-tails).

During the map study of the PF area, some general seafloor feature assemblages have been categorized. The main observed assemblages are: 1) lineations (both MSGLs and crag-and-tails) together with moraines;

2) rough bedrock with meltwater channels; mainly seen in the northern parts; and 3) long and densely packed MSGLs together with iceberg ploughmarks (Figure 9).

TABLE 2 Variation and occurrence of small-scale seafloor landforms in the PF area. All eight feature types identified have been counted and when applicable also described with orientation, areal coverage in % of total area, and/or length in km for linear forms.

Seafloor type	Number of identified features	Orientation	Areal coverage by % of total area	Length in km
<i>Bedrock outcrop</i>	87	-	-	-
<i>Iceberg ploughmarks</i>	402	Random	-	1-9
<i>MSGL</i>	105	NW-SE; N-S; SW-NE	-	1-21
<i>Crag-and-tail</i>	71	SW-NE; N-S	-	1-5
<i>Moraine</i>	15	NNW-SSE	-	3-36
<i>Meltwater channel</i>	52	NNW-SSE	3.8%	1-24
<i>GZW</i>	3	-	5.2%	-
<i>Rough bedrock</i>	3	-	23.6%	-

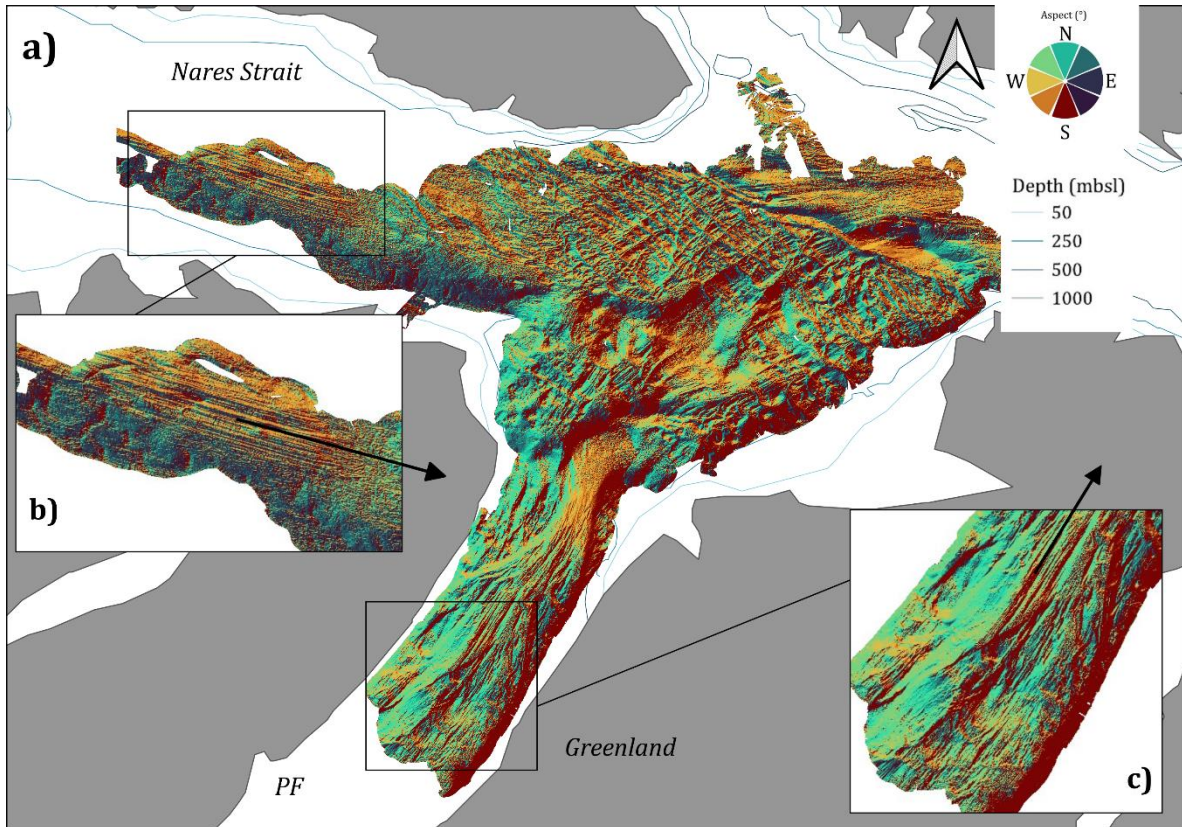


FIGURE 10 Aspect study of the PF and NS area. **a)** Overview of the main directions of landforms in the area. **b)** The NW part is dominated by NW-SE oriented lineations. **c)** The fjord sees mostly NE lineations.

The previously described main directions featured are again represented from the aspect study of the PF, showing that the principal directions of landforms are either NW-SE or N-S. The area described as rough bedrock shows a crisscross-like pattern in the aspect map (Figure 10).

4.2 Sherard Osborn fjord

The studied SOF area is around 1050 km² large in extent. Overall, the bathymetric layout of the fjord is characterized by a BS (hereafter the inner BS) in the landward part of the area as well as another BS (outer

BS) at the seaward side, where the fjord opens out into the Lincoln Sea (Figure 11). Between the two BSs there is a deeper part with smooth seafloor, covering most of the SOF area. The inner BS is shallow with depths of between 350 and 200 mbsl. Its surface is smooth, and it covers an area of just above 68 km², making up 6.5% of the total. The outer BS is rough-textured and slightly shallower, with depths between 400 and 150 mbsl. It covers an area of 100 km², which is 9.5% of the total SOF area. Between the two BSs, the seafloor is mostly around 800 mbsl in depth and smooth in its surface.

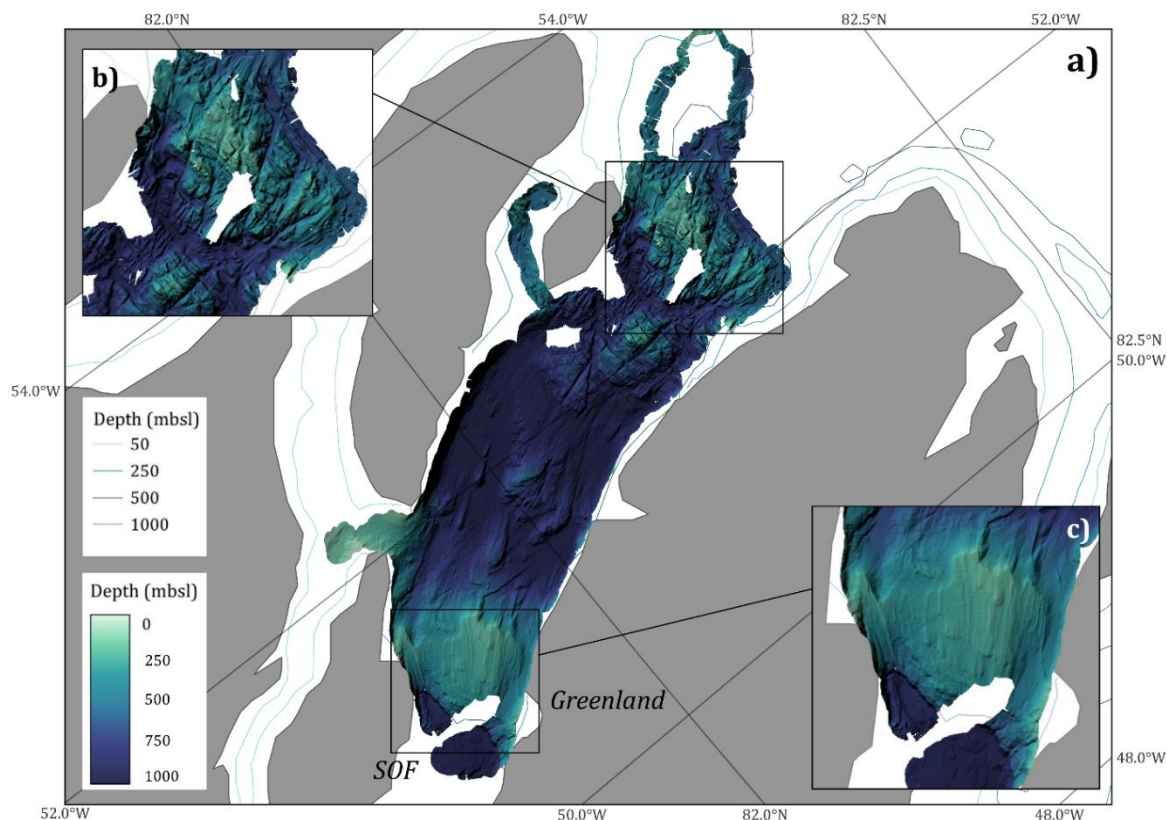


FIGURE 11 Bathymetric overview of the Sherard Osborn fjord, where the Ryder glacier drains. **a)** The map is projected to EPSG:3996 EGS 84 IBCAO Polar Stereographic. Darker blue and purple areas are deeper, and lighter blue and green colors are shallower. Blue hued contours display water depth outside of the high-resolution area. **b)** The outer BS with its rough bedrock topography. **c)** The inner BS at the mouth of the fjord.

The southern part of SOF characterized by the inner BS also sees some moraines in a NW-SE direction (Figure 12). On top of the inner BS, interpreted as a GZW of depositional origin, both MSGs and iceberg ploughmarks can be found. The iceberg ploughmarks are confined to the shallower parts of SOF. They are 1 - 4 km in length and in random orientation. The MSGs are oriented along the northward direction of the fjord. All the observed MSGs within SOF are in lengths of 1 - 4 km, with the median at 1 km and mean at 1.6 km. Slightly northwards, in the flatter and deeper section of SOF, the seafloor landforms are mostly of linear nature. Crag-and-tails and MSGs are both present in the NE direction of the fjord. The crag-and-tails are in general longer than the MSGs, with a length span of 1-6 km, its mean at 1.8 km and median length at 2 km. Multiple moraines are identified in the area, close to each other (Figure 12c). The SOF moraines see lengths between 1 and 27 km, with a mean length at 5.3 km and a median

at 4 km. An area at the southern end of the SOF is uncharted, right in the middle of two parallel moraines. It is not unlikely that these would be continuous and longer if the dataset was complete (Figure 12d).

The middle-to-northern area of SOF is dominated by meltwater channels and rough bedrock. The meltwater channels are in varied orientations, with some observed preference for N-S and NW-SE directions. They range in length from around 2 to at most 8 km and are generally 200 - 600 m in width. Some broader segments reach 800 m wide. The seafloor type categorized as rough bedrock is seen mostly in the middle of SOF between the moraines and the meltwater channel dominated area, and underneath the meltwater channels (Figure 12b). The latter being also described as the outer BS in previous literature (Jakobsson *et al.* 2020b; O'Regan *et al.* 2021). Its total combined area is 230 km², equivalent to 21.9% of the total SOF area (Table 3).

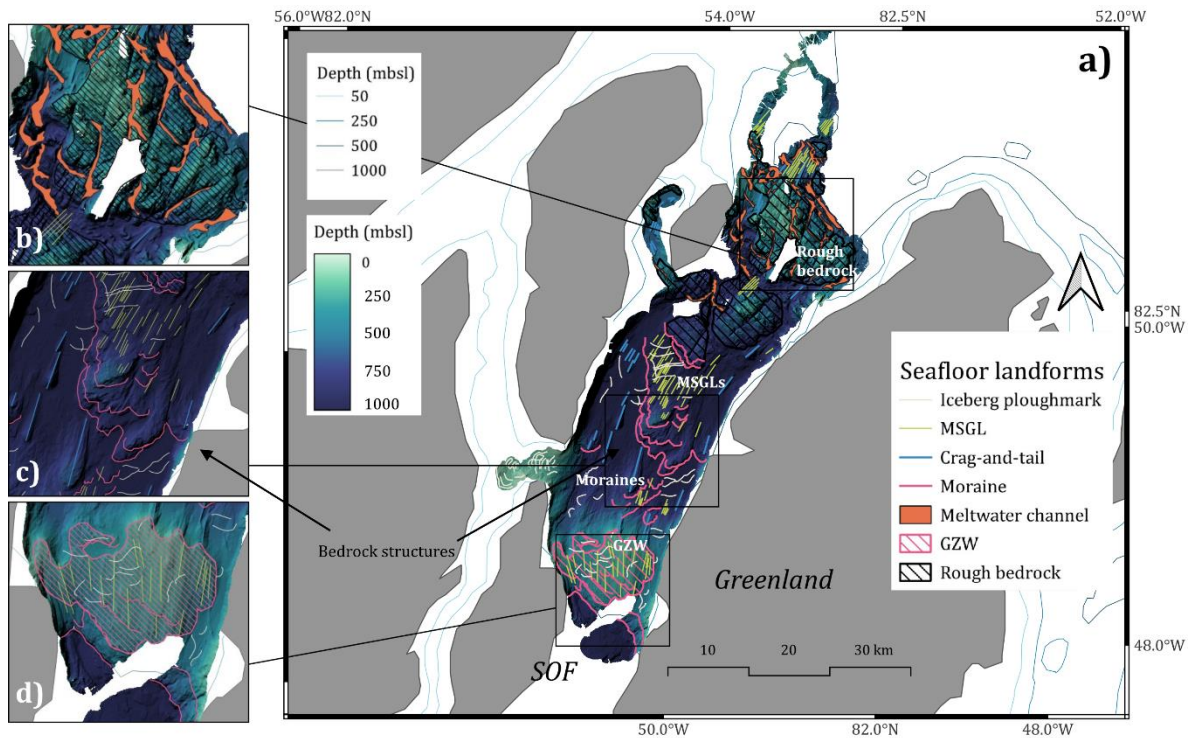


FIGURE 12 Identified seafloor landforms of SOF. **a)** Overview of the seafloor landform assemblages of SOF. **b)** An area dominated by rough bedrock with meltwater channels from the northern part of SOF, acting as the outer BS. **c)** Moraine ridges and lineations of the middle SOF. Some of the features here described as moraines are in fact bedrock structures as pointed out in the map. **d)** The GZW/ inner BS with superimposed MSGLs and iceberg ploughmarks of the fjord entrance.

The main assemblages found in SOF are: 1) GZW with iceberg ploughmarks; and 3) linear forms together with moraines; 2) rough bedrock with meltwater channels.

TABLE 3 The different types of seafloor landforms identified within SOF. Where suitable, area or length as well as orientation of landforms are stated.

Seafloor type	Number of identified features	Orientation	Areal coverage by % of total area	Length in km
<i>Iceberg ploughmarks</i>	62	Random	-	1-4
<i>MSGL</i>	109	SW-NE; N-S	-	1-13
<i>Crag-and-tail</i>	33	SW-NE; N-S	-	1-6
<i>Moraine</i>	25	NNW-SSE; W-E	-	1-27
<i>Meltwater channel</i>	27	N-S; NW-SE	3.4%	1-8
<i>GZW</i>	1	-	6.5%	-
<i>Rough bedrock</i>	5	-	21.9%	-

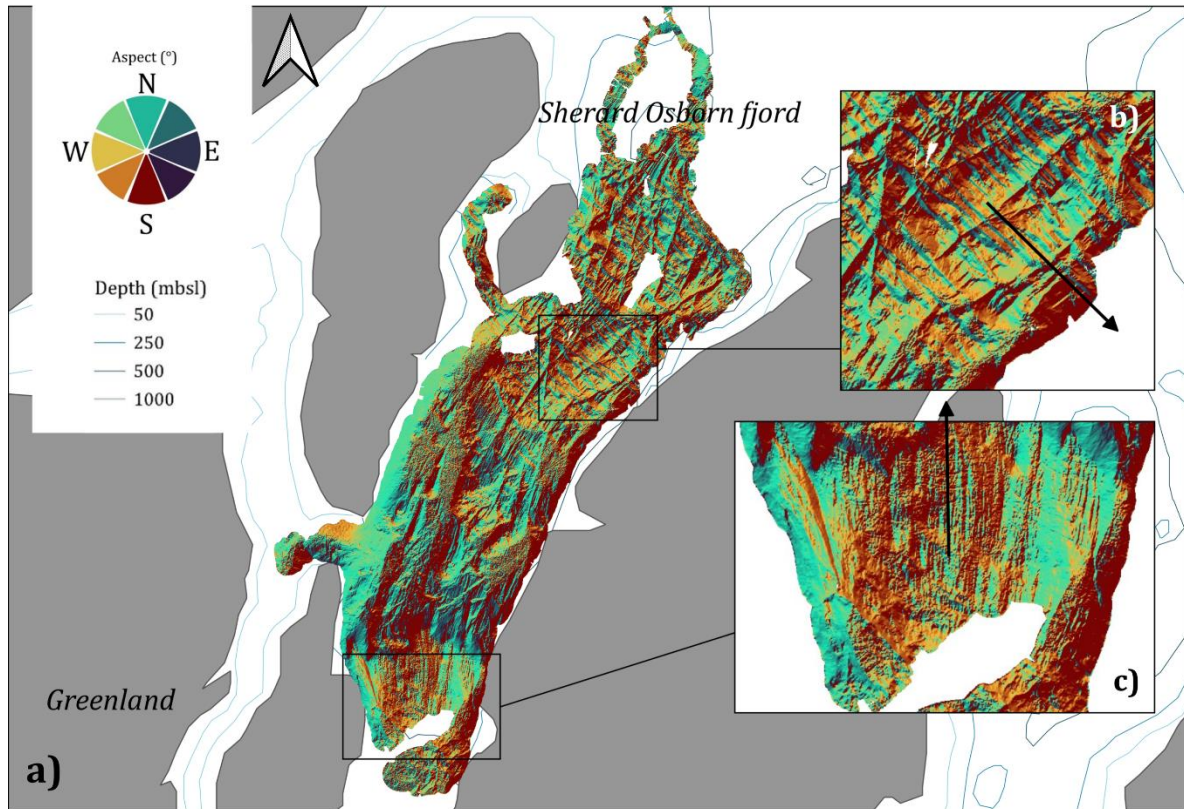


FIGURE 13 Aspect map of the Sherard Osborn fjord, displaying the direction of slopes in the area. **a)** An overview of the aspect study of SOF. **b)** The central-northern part of SOF sees NNW-SSE lineations in the aspect study. **c)** The southern part of the fjord is characterized by lineations in a northern direction.

From the aspect study of SOF (Figure 13), the abovementioned directions are seen. Within the southern part, the direction is N-S (Figure 13c). Further north, the lineations curve slightly to the eastern side, following along the curvature of the fjord. The northern part has a rougher texture, with two main directions identified, perpendicular to each other (Figure 13b). This is the rough bedrock as described above.

4.3 Victoria fjord

The multibeam bathymetry covers some of the Victoria fjord, as well as the adjacent

Nordenskiöld fjord in the east and parts of the Lincon Sea in the north (Figure 14). The entire area, in this paper described as VF, but also covering some of adjacent Nordenskiöld fjord, covers 1.43 km². Overall, VF contains few different types of identifiable landforms, with much of its area made up of rough bedrock (Figure 14). No GZW or BS of other type has been identified within the area. Much of the area is around 400-700 mbsl in depth (Figure 14). The deeper parts are deeper than 1000 mbsl.

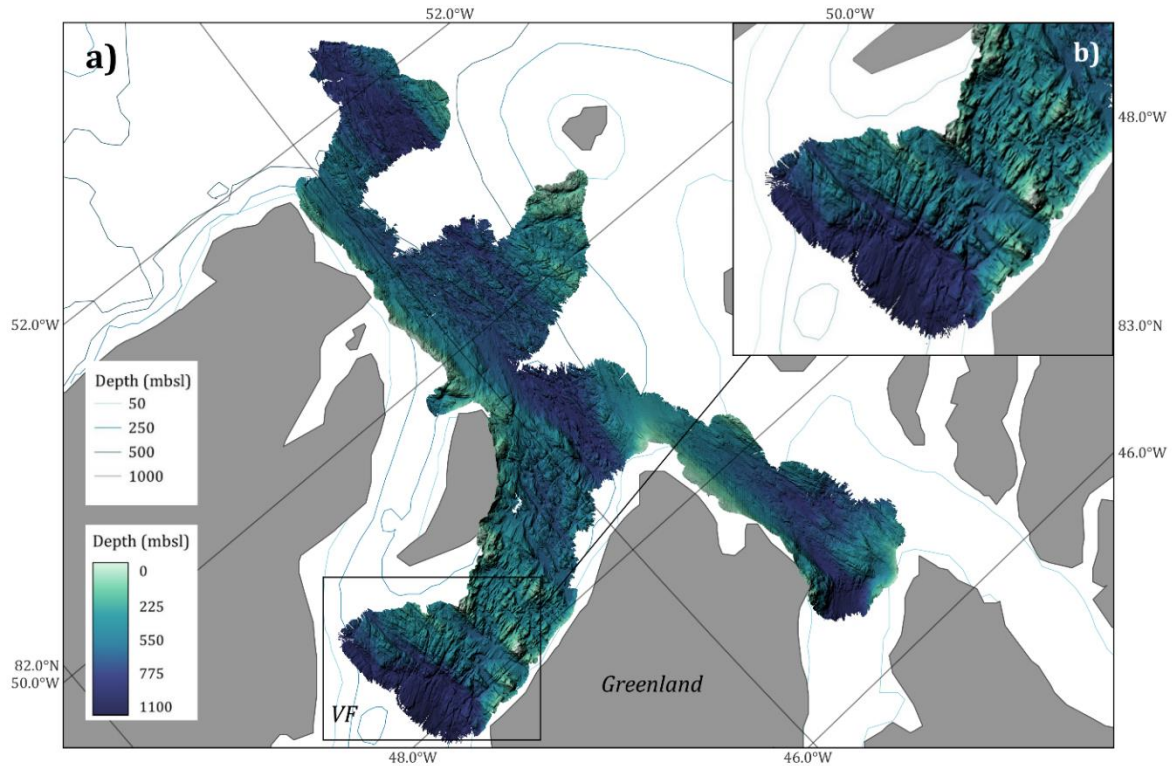


FIGURE 14 Bathymetric overview of Victoria fjord. **a)** Dark blues and purples display deeper parts. The shallower areas are shown in lighter blues and greens. The map is projected to EPSG:3996 EGS 84 IBCAO Polar Stereographic. Depth outside of the high-resolution area are displayed as contours of different blue hues. **b)** The rough-textured seafloor at the entrance to the Victoria fjord.

The rough bedrock is spread out over much of VF, especially prominent in the southern and middle parts (Figure 15). It covers a total of 0.48 km², corresponding to 33.6% of the total VF area. It has not been mapped as one continuous area, as the rough bedrock is broken up into parts by small sections of more sediment-dominated areas with linear bedforms and meltwater channels (Figure 15d). Through the central axis of the VF area, there is an elongated section in the NW-SE direction characterized by linear bedforms, both MSGs and crag-and-tails (Figure 15c). The area coincides with a deeper seafloor.

The MSGs of VF vary in length between 1 and 6 km. The median length is 3 km, and the mean is 2.9 km. Within the actual VF, the MSGs are oriented in a N-S direction. The rest of the VF area has MSGs oriented in a NW-SE direction. Crag-and-tails are found at mostly the same sites within VF as the MSGs. They appear primarily in the mid-section of the VF area, some having a similar

orientation as well. The crag-and-tails are between 1 and 3 km in length, with the mean length being 1.4 km and the median length 1 km. There is a band of crag-and-tails along the central axis of the VF area, with closely spaced crag-and-tails. This band is found between two sections of mostly MSGs, which also coincide with shallower seafloor.

Within, as well as in-between areas of rough bedrock, meltwater channels are present (Figure 15b). The channels of the northern part of VF are in clear NW-SE direction.

Further south, the meltwater channels are slightly more N-S, though some of the abovementioned direction is seen. The southernmost meltwater channels again have the NW-SE orientations. The meltwater channels are typically in lengths of 2-10 km, with some reaching 12 km and more. They are between 300 and 800 m wide, with some narrower and some wider sections present as well (Table 4).

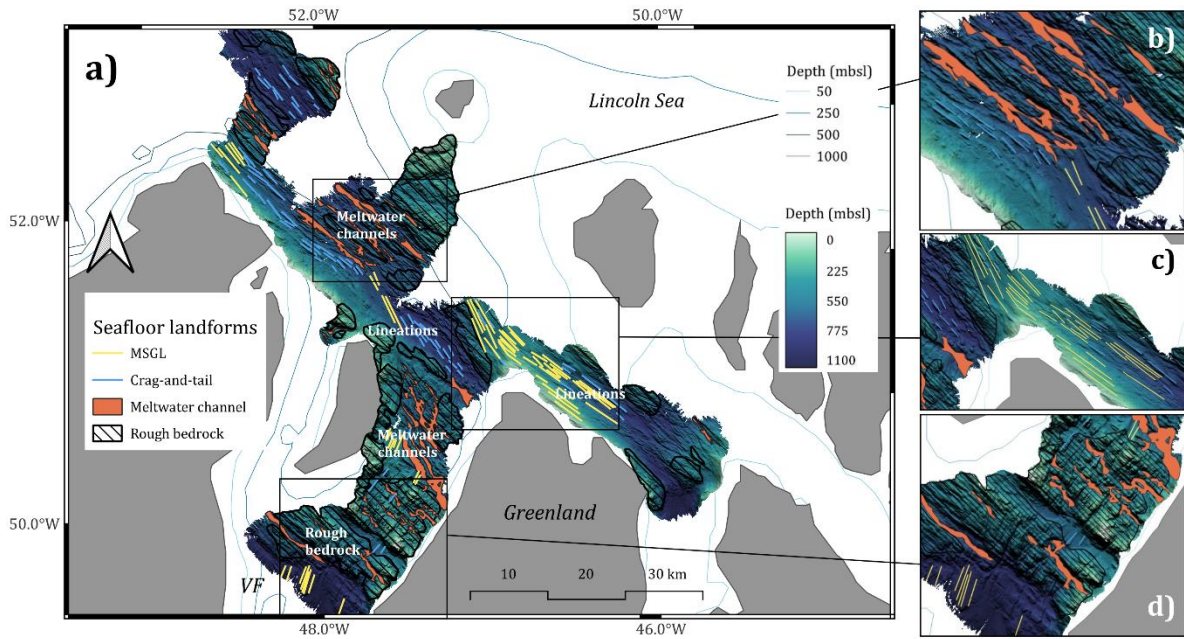


FIGURE 15 The observed landforms of VF. **a)** Overview of VF and its different landforms assemblages. **b)** Some of the northern area is dominated by rough bedrock and meltwater channels. **c)** Part of the eastern site is characterized by lineations, mainly MSGLs, but crag-and-tails are seen as well. **d)** The fjord mouth, dominated by rough bedrock.

Within VF, the following landform assemblages have been defined: 1) linear landforms, both crag-and-tails and MSGLs in

proximity to each other; and 2) rough bedrock with meltwater channels.

TABLE 4 The variation and sizes of identified seafloor landforms in the VF area. Landform orientation and sizes have been included where applicable.

Seafloor type	Number of identified features	Orientation	Areal coverage by % of total area	Length in km
<i>MSGL</i>	59	NW-SE; N-S	-	1-6
<i>Crag-and-tail</i>	76	NW-SE; N-S	-	1-3
<i>Meltwater channel</i>	46	NW-SE	5.8%	2-12
<i>Rough bedrock</i>	25	-	33.6%	-

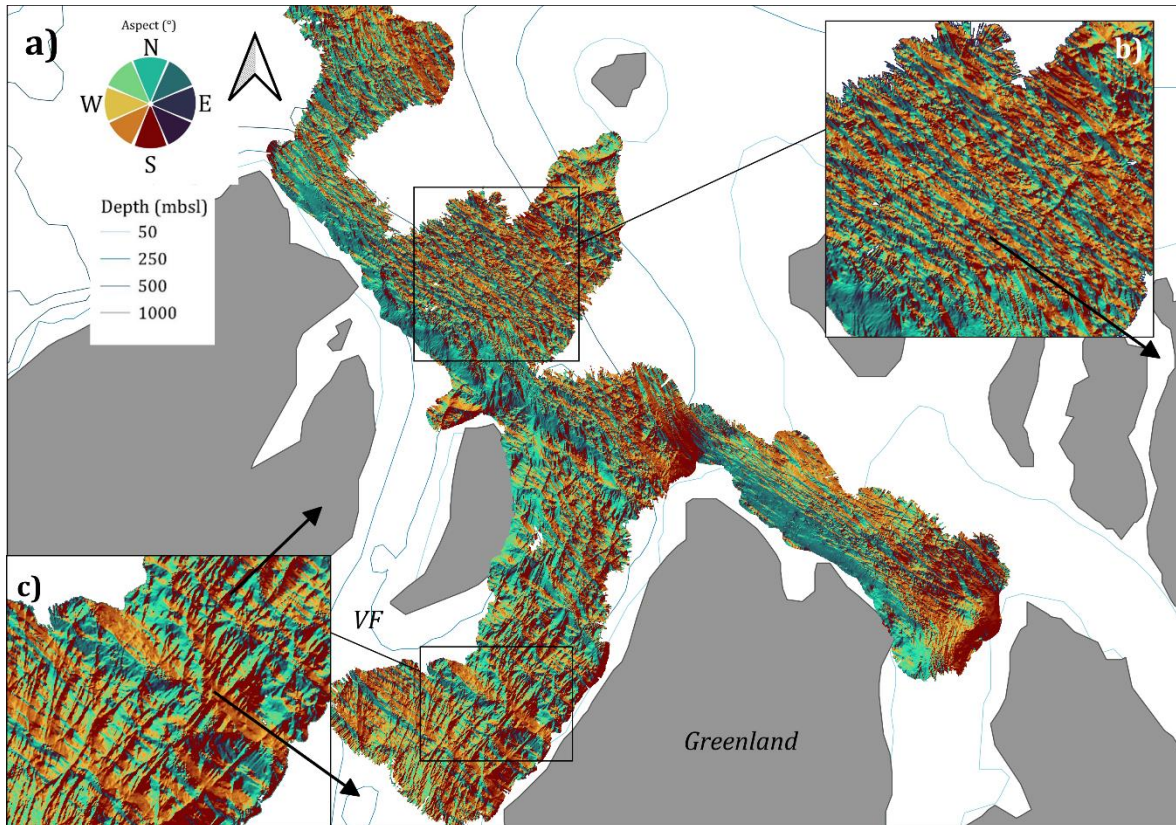


FIGURE 16 Aspect map of the Victoria fjord. **a)** Overview showing the directional variations found in VF and the surrounding area. **b)** One of the main directions in the area is NW-SE found in the seaward side of the fjord. **c)** The fjord opening has two main directions: one is the same as in **b)**, the other is perpendicular to the first.

The aspect study of VF (Figure 16) shows much of the area as rough bedrock with multidirectional lineations, often seen as perpendicular to each other. In the southeastern side of the VF area, some of the NW-SE orientation of the lineations is seen.

4.4 Bathymetric profiles

The bathymetric profiles drawn between the innermost and outermost points of the fjords, utilizing the available high-resolution dataset, were saved as xyz points and plotted using the Python library Matplotlib (Figure 17). Some parts of the SOF and VF lines lack depth data, breaking up the profiles (Figure 17).

The PF profile starts at a depth of around 1000 mbsl in the deep inner part of the fjord (Figure 17c). Around 8000 m seawards, it deepens to between 1100 and 1200 mbsl, remaining within that interval until around 35 000 m seawards, where the GZW, also described as a BS, is found. The depth decreases steadily to around 400 mbsl on the BS. This is followed by a small increase in depth by approximately 100 m at 50 000 m out, after which the area becomes shallower, reaching its shallowest point along the profile line at 250 mbsl on the outer GZW. The location of the outer GZW is approximately 6000 m from the starting point. Beyond the outer GZW, the seafloor roughens in texture as it gradually deepens to around 800 mbsl at around 80 000 m out.

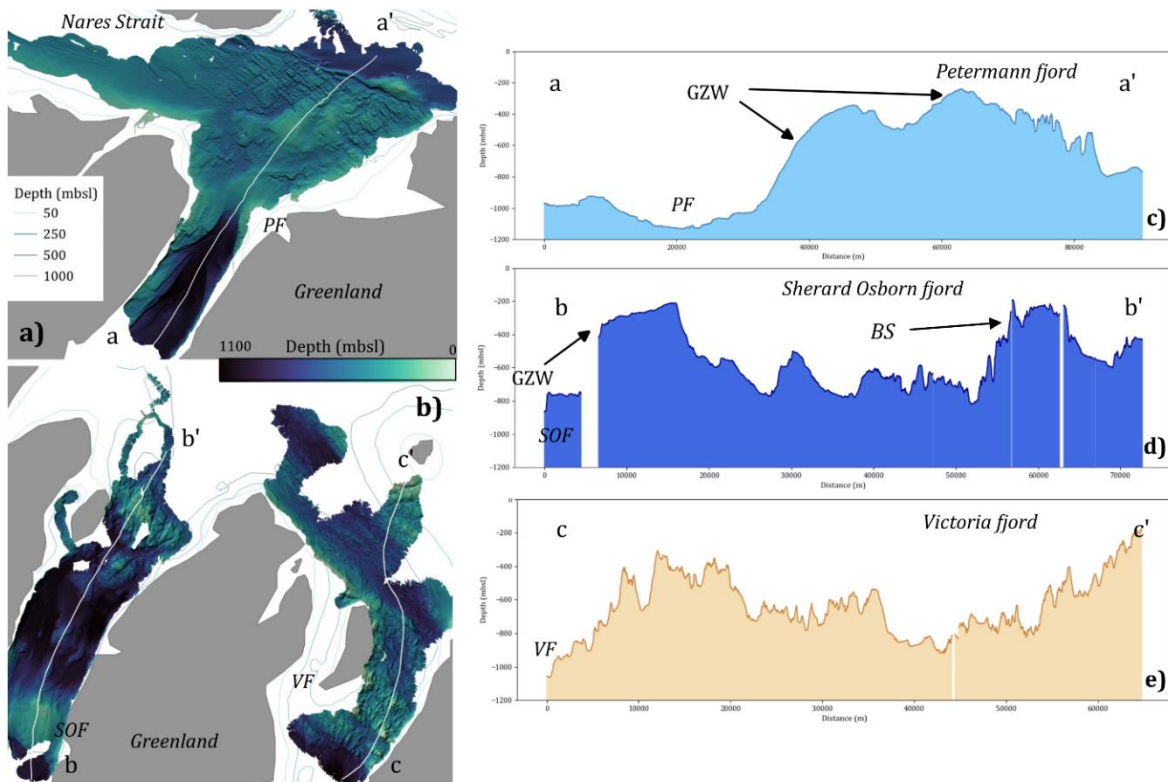


FIGURE 17 Placement of profile lines in the different fjords as well as their corresponding bathymetric profiles. They are displayed as VF in tan, PF in light blue, and SOF in darker blue **a)** The PF profile from the inner fjord through both GZWs. **b)** Profile lines for SOF and VF, following assumed circulation patterns. **c)** Terrain profile of PF with GZWs. **d)** The SOF profile with its GZW (inner BS) and outer BS. **e)** The VF terrain profile with its rough topography.

The SOF starts at a depth of 800 mbsl, remaining at this depth until reaching a steep shallowing to 400-200 mbsl at around 10 000 m from the start. This is the inner BS, also named the GZW due to previously interpreted differences in the nature of the two BSs of SOF. Seawards of the GZW, the fjord deepens again to depths of around 800-600 m with some sinuosity in its height variation. This pattern is maintained until almost 60 000 m out from the starting point, where there is another shallow area. Depths here are around 200 mbsl, being the outer BS. Its surface is rougher in texture than the surface of the inner BS. At 65 000 m outwards, the outer BS tapers off and SOF deepens again by about 200 m.

The VF profile begins at its deepest point of about 1100 mbsl. The depth profile steadily shallows over the following 10 000 m, with an irregular variability. At 10 000-20 000 m away from the start, there is a shallower area with depths of around 400 mbsl. Northwards of this, there is a deepening to a stable section of the profile at approximately 600 mbsl until around 35 000 m from the start. At this point, there is another deepening of around 200 m. This is maintained until nearly 55 000 m out, after which a continuous shallowing is present until the shallowest depth observed of around 200 mbsl at the northernmost point along the profile line.

5 Discussion

The aim of this study is the comparison between the submarine geomorphology of the three adjacent northern Greenland fjords, Petermann fjord, Sherard Osborn fjord, and Victoria fjord, in relation to their respective floating ice tongue extents. The following two questions were asked: 1) What different submarine landforms and landform assemblages can be observed in the three adjacent fjords? and 2) Are there observed differences in the fjords' bottom topographies that explain variations in ice-tongue melting and stability among the three outlet glaciers?

5.1 Observed landforms

Within the three adjacent fjords, a multitude of submarine geomorphological landforms have been identified and mapped. Those categorized as glacial landforms have been classified.

The three fjords all host glacial landforms of subglacial origin: glacial lineations, both MSGs and crag-and-tails, as well as meltwater channels. Subglacial landforms were formed beneath the ice sheet within its area of extent. Since Greenland was entirely ice-covered during the LGM (Englund 1999), the presence of subglacial landforms at this site is to be expected. Ice-marginal landforms, such as different types of end moraines and GZWs, were formed at the ice-marginal site during the retreat and standstills of the ice sheet. Such landforms have been identified within the PF and SOF areas, but not within the VF area. Previous morphological studies of the site have also identified ice-marginal landforms within PF and SOF. Especially the GZWs, found in both fjords, have been documented and described (Jakobsson *et al.* 2018; Jakobsson *et al.* 2020b). In both PF and SOF, moraines have been identified within the shallower and the deeper parts. As no previous studies focusing on submarine landforms within VF have been published, direct comparisons are not possible. Glaciomarine landforms, namely iceberg ploughmarks, have been

identified within PF and SOF areas in large numbers. The iceberg ploughmarks were formed from the abrasion of seafloor from floating icebergs. These were formed after the retreat of the GrIS. Iceberg ploughmarks have been found exclusively within the shallower parts of PF and SOF, superimposed on for example GZWs. The deeper parts, with depths of more than 1000 mbsl, were likely too deep for the floating icebergs to reach the seafloor.

5.2 Controls on ice tongue melting

Within the PF area including NS, the ice flow direction has been interpreted as two-directional, indicating an overlapping flow. The main direction is SW-NE, in which glacial lineations have been identified (Figure 10). Moraines perpendicular to this direction are seen, both within the fjord and outside of the BS (Figure 9). The other ice flow direction is following the path of the NS, in an approximately SSE-NNW direction. MSGs in this direction are longer than those in the fjord direction, indicating a faster flow rate or a longer time of flow (Livingstone *et al.* 2016). The SOF area does not show the same signs of an along the Greenland coast flow, though it can be assumed that this direction is present outside of the dataset location. Within the SOF, the ice flow is interpreted as along the fjord, similar to the PF, shown by the direction of glacial lineations (Figure 12). Due to the curvature of the fjord, such curvatures are also observed in the lineations.

Within the VF area, the NS direction of the ice flow, following the contour of the northern coast of Greenland, is most obvious in the direction of the lineations (Figure 15) as well as the aspect study (Figure 16). Some lineations following the direction of the fjord can be seen at the southernmost part of the VF area, though more bathymetric data from within the fjord would be required to truly make such connections.

From the length variation of MSGs within PF, and the strong presence of NW-SE directions within VF, it can be interpreted that the along-coast ice flow was faster and dominant over the internal fjord flows.

The flow of the GrIS is strongly connected to supply of sediments and till, as the glacier transports eroded materials, depositing them at its site of termination. Given the inferred high flow rate along the NS, and the less frequent presence of perpendicular moraines, sediment deposition from this ice stream was assumed minimal. This ice stream likely had a termination site with deposits elsewhere. Hence why the northernmost parts of both PF and SOF are mostly covered in rough bedrock with little to no sediment coverage. The PF and SOF areas have shallower and smoother areas, assumed to be sediment covered, landwards and within the fjords. This is where the ice flow is assumed to be mainly in the along-fjord directions, containing ice carried from their glaciers, PG and RG respectively. These two glaciers seem to have had multiple standstill periods during their retreats, when there was enough time for greater depositions of materials at the termination sites, for example resulting in the observed GZWs. According to previous studies, GZWs have control over the inflow of water, acting as BSs at the fjord mouths (Jakobsson *et al.* 2020b; Johnson *et al.* 2011; Reilly *et al.* 2019), in this case hindering the entrance of warmer NA water masses.

The VF area sees no such depositional landforms. Most of its seafloor is rough bedrock with minimal sediment presence. Some of the shallower parts of VF, where the surface is smoother and there are MSGs, seem to have a sediment layer covering the bedrock. MSGs are assumed to be sediment-dependent landforms (Livingstone *et al.* 2016).

The geomorphological differences between the three fjords are most apparent in the varied presence of depositional landforms. While the PF and SOF areas have significant amounts of sediment, with accompanying sedimentary landforms such as MSGs, GZWs and iceberg ploughmarks, the VF area

is almost void of such landforms. Besides the MSGs present in the VF area, its seafloor is greatly dominated by rough bedrock.

These apparent differences can be compared with the geology of the area and the ice stream flows. The geologies of and around the three fjords are similar in their components (Figure A1 in Appendix). The different sediment distribution is likely not explained by different bedrock properties. Instead, it may be due to the differences in ice stream flows. Figure 5 displays the ice stream velocities of all GrIS ice streams. Out of the three glaciers, the PG has a noticeably more rapid flow than the other two. The RG ice stream flow is the second fastest, with the OFG flow being the slowest and smallest of the three. It can thus be assumed that the sediment supply from inland Greenland is the greatest in PF and the poorest in VF. Assuming the ice stream flow rate relationship between the three glaciers has not changed significantly since the LGM, this could indicate that one of the most important controlling factors on the fjords' floating ice tongue extents is their respective glaciers' sediment supply. PF, which sees the greatest ice stream flow, also has the highest presence of depositional landforms and the longest floating ice tongue. SOF, which has the second-greatest ice stream flow of the three, also has a great number of depositional landforms and a remaining ice tongue, though a shorter one than the PF. The VF ice tongue is almost completely collapsed, which could be related to its lack of depositional landforms to hinder the entrance of warm NA water. The slow flow rate of the OFG may be the reason for its low sediment coverage. The retreat of the GrIS within the VF area during the LGM may also have been too rapid, without longer standstill periods allowing for a buildup of material to form GZWs. Since the VF has no identifiable BS, the NA water can more easily flow into the fjord, interacting with the terminating glacier, melting it from below as well as inducing iceberg calving. Likely for this reason, the floating ice tongue collapsed almost entirely during the beginning of the 21st century. Though this would require

more data from the inner parts of the fjord to understand better.

Both PF and SOF have also seen significant melting of their ice tongues, both from continuous retreat and from catastrophic calving events during the 20th and 21st century (Johnson *et al.* 2011; Jakobsson *et al.* 2020b). While the PG has had an average ice tongue retreat of 311 m/yr between the years 1948 and 2015. For the same period, the RG ice tongue retreated at a noticeably slower pace of 43 m/yr (Hill *et al.* 2017). This great difference in retreat rate could be explained by the two BSs of SOF compared to only one in PF. For this reason, the RG ice tongue was likely better protected from the inflow of warm NA water. This has been described in previous studies as well (Jakobsson *et al.* 2020b; O'Regan *et al.* 2021).

Since 2015, the PG has experienced a slight advance of its ice tongue. This can be identified when comparing satellite images of the current ice extent with the extent of bathymetric data from 2015. Where there was no ice and MBES data could be collected onboard IB Oden in 2015, the current ice margin lies above. PG also has an overall longer floating ice tongue than SOF. Since PF is the furthest from FS, it may be that less of the warm NA water reaches it compared to VF and SOF, situated closer to the NA water path. VF, being closest to FS of the three, may be exposed to more warm water for that reason as well, which may provide yet another explanation for why so much more of its ice tongue has retreated already.

5.3 Study limitations

Considering the difficult-to-reach position of the northern Greenland fjords of this study, there is some difference in the data availability of the three fjords. While the SOF area covers much of the actual fjord, the PF area does not reach as far into the fjord due to the ice tongue preventing entrance with IB Oden. Because of sea ice, the VF area contains even less of the actual fjord, as moving further into the fjord proved

impossible. There are also some data gaps within the data sets, most noticeable for the VF area where parts remain uncharted.

Another limitation to the study is that of inconsistencies in bathymetric resolution. The PF and SOF areas are covered by bathymetric data gridded at a 15 x 15 m resolution, while that of the VF area is 30 x 30 m. For this reason, some of the analysis of the method, most of which was performed in QGIS, required slightly different handling of the VF data compared to the other two. Some tweaking of the settings was necessary to ensure the best possible understanding and interpretation of the VF geomorphology. Additionally, the lack of previous research focused on VF creates uncertainties as there is no way to make direct comparisons between interpretations made in this study and previous work.

The study being based exclusively on multibeam bathymetry without considering other types of geophysical data is a third limitation. While high-resolution multibeam bathymetry gives good two-dimensional indications of seafloor structures, it does not provide any insights below surface. Hence, it cannot be said with certainty that landforms interpreted as sedimentary may not in reality be bedrock structures.

5.4 Broader implications and future research

This study has focused exclusively on the AO region, specifically northern Greenland and the three adjacent fjords. Though the geographical extent is limited, some of the findings may be applicable to other marine terminating glaciers as well. These can be found all around Greenland as well as Antarctica, the two sites for continental ice sheets. The study findings point to the importance of one or more BS to hinder the inflow of warmer water to the fjord, which may cause melting of the floating ice tongues. This in turn poses a serious climate issue, as the albedo provided by the light ice is necessary for reflecting incoming solar radiation to keep Earth's climate from

overheating. Melting of the GrIS, which contains great masses of ice, may also lead to a noticeable increase in global sea levels, which has the risk of drowning coastal areas, impacting both human and non-human terrestrial life.

The study shows that the presence of sedimentary structures can provide necessary control of the water inflow, allowing the fjord water temperatures to remain cold and the ice to keep from retreating. While differences in bedrock structures, whether more or less erosive, may influence the sediment supply to the fjords, the main difference seems to be due to ice stream flow rates. With greater ice stream flow, the glacier is likely to carry with it more material to be deposited at the termination site, which will then build up sedimentary structures such as GZWs that may prevent the inflow of warm water.

6 Conclusions

The first question asked was regarding landforms in the northern Greenland fjords. The three studied fjords have seafloors strongly characterized by landforms of glacial origins. Subglacial landforms, which are formed underneath the moving ice sheet, such as MSGs and crag-and-tails, have been identified within all three fjords. Ice-marginal landforms, which are created at past ice margin sites, have been identified with PF and SOF, but appear to be nonexistent within the VF area, which is dominated by rough bedrock. Glaciomarine landforms, namely iceberg ploughmarks, were identified within PF and SOF where the seafloor is shallow and more sediment laden. The VF area instead lacks visible iceberg ploughmarks, likely due to its rough texture.

The varying seafloor morphologies of the fjords correspond to differences in their floating ice tongue stability and retreat rates, answering the second question. While the PF has the longest remaining ice tongue

While it is difficult if not impossible to manually control the sediment supply to prevent the melting of ocean terminating glaciers, it could perhaps be possible to engineer underwater dams or similar structures to synthetically carry out the effects of a BS. A major hindrance is the incredibly large scale of the fjords and the massive depths. Potential solutions to this would be an interesting topic for future research to embark upon, to see whether such structures could be crafted to prevent further melting of the floating ice tongues.

Additionally, it would be beneficial to continue using MBES and similar acoustic methods to acquire bathymetric data from the currently unmapped areas, as well as increase the resolution of already mapped sites. This would allow for more precise identification of seafloor landforms.

out of the three, it has seen a steadily high retreat of ice mass. The inner GZW, acting as a BS within the PF, prevents some of the warm water inflow. By comparison, SOF has seen a significantly slower ice tongue retreat, likely due to the presence of two BSs within the fjord, one made of sediments and the other of bedrock, hindering water inflow. VF, which has no noticeable BS and very little sediment, has almost no ice tongue remaining. It can be interpreted that the OFG's relatively low ice flow rate brings too little sediments for the buildup of a sedimentary BS within the fjord. This in turn leaves the VF vulnerable to the inflow of warm water.

On a broader scale, this study may contribute some knowledge on ice-ocean dynamics. As global temperatures rise in direct response to human activity, an improved understanding of ice-ocean interaction is critical for predicting future ice loss and global sea level rises, as well as decrease in albedo.

7 Acknowledgements

I thank my supervisor Professor Martin Jakobsson for giving me this opportunity as well as assisting me in my study throughout the process. Providing me with thorough and helpful feedback, insightful comments, and not least great amounts of inspiration. As an authority on the subject, his insights have been of utmost value. Professor Jakobsson is also the one who first introduced me to the field of marine geology, of which I feel very grateful.

I also want to thank Dr Sarah Greenwood, who was kind enough to meet with me and offer her expertise in glacial morphology. Getting her insights and interesting questions on my study helped me in reaching my conclusions.

I would lastly like to thank Dr Richard Gyllencreutz who has been continuously helpful and very supportive of me delving into this field.

8 References

References have been divided into 7.1 Literature, used primarily in 2 Background and 5 Discussion sections of the paper, and 7.2 Data sources from where bathymetric grids, geological data, and datasets have been acquired.

8.1 Literature

Batchelor, C.L., Dowdeswell, J.A. & Ottesen, D., 2018. Submarine Glacial Landforms. In: Micallef, A., Krastel, S., Savini, A. (eds) Submarine Geomorphology. Springer, Cham: Springer Geology.

Beckmann, J. & Winkelmann, R., 2023. Effects of the extreme melt events on ice flow and sea level rise of the Greenland Ice Sheet. *The Cryosphere*, 17. <https://doi.org/10.5194/tc-17-3083-2023>

Bennet, M.R., 2002. Ice streams as the arteries of an ice sheet: their mechanics, stability and significance. *Earth Science Reviews*, 61(3-4). [https://doi.org/10.1016/S0012-8252\(02\)00130-7](https://doi.org/10.1016/S0012-8252(02)00130-7)

Cochran, J.R., Edwards, M.H. & Coakley, B.J., 2006. Morphology and structure of the Lomonosov Ridge, Arctic Ocean. *Geochemistry, Geophysics, Geosystems*, 7(5). <https://doi.org/10.1029/2005GC001114>

Cook, J., n.d. Atlantic and Arctic Ocean currents. Woods Hole Oceanographic Institution. <https://www.whoi.edu/multimedia/atlantic-arctic-currents/> [accessed 19 December 2024].

de Steur, L., n.d. The Fram Strait Arctic Outflow Observatory. Norsk Polarinstitut. <https://www.npolar.no/en/projects/fram-strait-arctic-outflow-observatory/> [accessed 8 December 2024].

Elmes, A., Levy, C., Erb, A., Hall, D.K., Scambos, T.A., DiGirolamo, N. & Schaaf, C., 2021. Consequences of the 2019 Greenland Ice Sheet Melt Episode on Albedo. <https://doi.org/10.3390/rs13020227>

Englund, J., 1999. Coalescent Greenland and Innuitian ice during the Last Glacial Maximum: revising the Quaternary of the Canadian High Arctic. *Quaternary Science Reviews*, 18(3). [https://doi.org/10.1016/S0277-3791\(98\)00070-5](https://doi.org/10.1016/S0277-3791(98)00070-5)

Furlotti, A., 2024. 3D-Modelling of Ice Dynamics at C.H. Ostenfeld Glacier, Northern Greenland. Stockholm University.

Harris, P.T., Macmillan-Lawler, M., Rupp, J. & Baker, E.K., 2014. Geomorphology of the oceans. *Marine*

Geology, 352. <http://dx.doi.org/10.1016/j.margeo.2014.01.011>

Hill, E.A., Carr, J.R. & Stokes, C.R., 2017. A Review of Recent Changes in Major Marine-Terminating Outlet Glaciers in Northern Greenland. *Frontiers in Earth Science*, 4(111). <https://doi.org/10.3389/feart.2016.00111>

Hill, E.A., Carr, J.R., Stokes, C.R. & Gudmundsson, H., 2018. Dynamic changes in outlet glaciers in northern Greenland from 1948 to 2015. *The Cryosphere*, 12(3243-3263). <https://doi.org/10.5194/tc-12-3243-2018>

Hogan, K.A., Jakobsson, M., Mayer, L., Reilly, B.T., Jennings, A.E., Stoner, J.S., Nielsen, T., Andersen, K.J., Nørmark, E., Heirman, K.A., [...] 2020. Glacial sedimentation, fluxes and erosion rates associated with ice retreat in Petermann Fjord and Nares Strait, north-west Greenland. *The Cryosphere*, 14(261-286). <https://doi.org/10.5194/tc-14-261-2020>

IHO, 2002. The Arctic Ocean and its Sub-Divisions. Limits of Oceans and Seas. 4th ed. draft.

Jakobsson, M., Andreassen K., Bjarnadóttir, L.R., Dove, D., Dowdeswell, J.A., England, J.H., Funder, S., Hogan, K., Ingólfsson, Ó., Jennings, [...] 2014. Arctic Ocean glacial history. *Quaternary Science Reviews*, 92. <https://doi.org/10.1016/j.quascirev.2013.07.033>

Jakobsson, M., Gyllencreutz, R., Mayer, L.A., Dowdeswell, J.A., Canals, M., Todd, B.J., Dowdeswell, E.K., Hogan, K.A. & Larter, R.D., 2016. Mapping submarine glacial landforms using acoustic methods. *Atlas of Submarine Glacial Landforms: Modern, Quaternary and Ancient*, 46. <https://doi.org/10.1144/M46>

Jakobsson, M., Hogan, K.A., Mayer, L.A., Mix, A., Jennings, A., Stoner, J., Eriksson, B., Jerram, K., Mohammad, R., Pearce, C., [...] 2018. The Holocene retreat dynamics and stability of Petermann Glacier in northwest Greenland. *Nature Communications*, 9(2018). <https://doi.org/10.1038/s41467-018-04573-2>

Jakobsson, M., Mayer, L., Farrell, J. & Ryder 2019 Scientific Party., 2020a. Expedition Report: SWEDARCTIC Ryder 2019. Luleå, Sweden: Swedish Polar Research Secretariat.

Jakobsson, M., Mayer, L.A., Nilsson, J., Stranne, C., Calder, B., O'Regan, M., Farrell, J.W., Cronin, T.M., Brüchert, V., Chawarski, J., [...] 2020b. Ryder Glacier in northwest Greenland is shielded from warm Atlantic water by a bathymetric sill. *Communications Earth & Environment*, 45(1). <https://doi.org/10.1038/s43247-020-00043-0>

Jakobsson, M. & Mix, A.C., 2015. EXPEDITION REPORT SWEDARCTIC Petermann 2015: Final Report

- Petermann 2015 Expedition Icebreaker Oden. Luleå, Sweden: Swedish Polar Research Secretariat.
- Johnson, H.L., Münchow, A., Falkner, K.K. & Melling, H., 2011. Ocean circulation and properties in Petermann Fjord, Greenland. *Journal of Geophysical Research: Oceans*, 116(C1).
<https://doi.org/10.1029/2010JC006519>
- Kongsberg, 2006. EM 122. Kongsberg Maritime AS.
- Livingstone, S.J., Stokes, C.R., Cofaigh, C.Ó., Hillenbrand, C.-D., Vieli, A., Jamieson, S.S.R., Spagnolo, M. & Dowdeswell, J.A., 2016. Subglacial processes on an Antarctic ice stream bed. 1: Sediment transport and bedform genesis inferred from marine geophysical data. *Journal of Glaciology*, 62(232).
<https://doi.org/10.1017/jog.2016.18>
- Marshall, S., 2005. Recent advances in understanding ice sheet dynamics. *Earth and Planetary Science Letters*, 240(2).
<https://doi.org/10.1016/j.epsl.2005.08.016>
- Mashayek, A., 2023. Large-scale impacts of small-scale ocean topography. *Journal of Fluid Mechanics*, 964(2023). <https://doi.org/10.1017/jfm.2023.305>
- Morlighem, M., Williams, C.N., Rignot, E., An, L., Arndt, E., Bamber, J.L., Catania, G., Chauché, N., Dowdeswell, J.A., Dorschel, B., [...] 2017. BedMachine v3: Complete Bed Topography and Ocean Bathymetry Mapping of Greenland From Multibeam Echo Sounding Combined With Mass Conservation. *Geophysical Research Letters*, 44. <https://doi.org/10.1002/2017GL074954>
- Münchow, A., Padman, L., Washam, P. & Nicholls, K.W., 2016. The ice shelf of Petermann Gletscher, North Greenland, and its connection to the Arctic and Atlantic Oceans. *Oceanography*, 29(4).
<https://doi.org/10.5670/oceanog.2016.101>
- NASA Earth Observatory, n.d. Topography of Greenland.
<https://earthobservatory.nasa.gov/images/5118/topography-of-greenland> [accessed 5 December 2024].
- NOAA National Oceanic and Atmospheric Administration, 2024. How many oceans are there?
<https://oceanservice.noaa.gov/facts/howmanyoceans.html> [accessed 5 December 2024].
- NOAA National Oceanic and Atmospheric Administration, 2009. How Multibeam Sonar Works.
<https://oceanexplorer.noaa.gov/explorations/09bermuda/background/multibeam/multibeam.html> [accessed 2025-01-22].
- Münchow, A., Falkner, K.K., Melling, H., Rabe, B. & Johnson, H.L., 2011. Ocean Warming of Nares Strait Bottom Waters: Off Northwest Greenland, 2003-2009. *Oceanography*, 24(3).
<https://doi.org/10.1038/s43247-022-00498-3>
- O'Regan, M., Cronin, T.M., Reilly, B., Olsen Alstrup, A.K., Gemery, L., Golub, A., Mayer, L.A., Morlighem, M., Moros, M., Munk, O.L., [...] 2021. The Holocene dynamics of Ryder Glacier and ice tongue in north Greenland. *The Cryosphere*, 15.
<https://doi.org/10.5194/tc-15-4073-2021>
- Rantanen, M., Karpechko, A.Y., Lipponen, A., Nordling, K., Hyvärinen, O., Ruosteenoja, K., Vihma, T & Laaksonen, A., 2022. The Arctic has warmed nearly four times faster than the globe since 1979. *Communications Earth & Environment*, 3(168).
- Reilly, B.T., Stoner, J.S., Mix, A.C., Walczak, M.H., Jennings, A., Jakobsson, M., Dyke, L., Glueder, A., Nicholls, K., Hogan, K.A., [...] 2019. Holocene break-up and reestablishment of the Petermann Ice Tongue, Northwest Greenland. *Quaternary Science Reviews*, 218(2019).
<https://doi.org/10.1016/j.quascirev.2019.06.023>
- Ruddiman, W.F., 2014. *Earth's Climate: Past and Future*. 3rd ed. New York: W.H. Freeman and Company.
- Rudels, B., Anderson, L., Eriksson, P., Fahrbach, E., Jakobsson, M., Jones, E.P., Melling, H., Prinsenberg, S., Schauer, U. & Yao, T., 2012. Observations in the Ocean, in: Lemke, P., Jacobi, H-W. (Eds.), *Arctic Climate Change: The ACSYS Decade and Beyond*. Springer, pp. 117-198. <https://doi.org/10.1007/978-94-007-2027-5>
- SCUFN (GEBCO Sub-Committee on Undersea Feature Names), n.d. Generic Term and Definition.
<https://scufn.ops-webservices.kr/new-generic-term-and-definition/> [accessed 2024-12-10].
- Skinner, B. & Murck, B.W., 2011. *The Blue Planet: An Introduction to Earth System Science*. 3rd ed. United States of America: John Wiley & Sons Inc.
- Stewart, H.A. & Jamieson, A.J., 2019. The five deeps: The location and depth of the deepest place in each of the world's oceans. *Earth Science Reviews*, 197(2019).
<https://doi.org/10.1016/j.earscirev.2019.102896>
- Talley, L., Pickard, G., Emery, W. & Swift, J., 2011. *Descriptive Physical Oceanography*. Oxford, UK: Elsevier Ltd.
- The GEOEO Shipboard Scientific Party, 2025. *GEOEO North of Greenland 2024: Expedition Report*. Luleå, Sweden: Swedish Polar Research Secretariat.
- Timmermans, M-L. & Marshall, J., 2020. Understanding Arctic Ocean Circulation: A Review of Ocean Dynamics in a Changing Climate. *Journal of Geophysical Research: Oceans*, 125(4).
<https://doi.org/10.1029/2018JC014378>
- Weatherall, P., Marks, K.M., Jakobsson, M., Schmitt, T., Tani, S., Arndt, J.E., Rovere, M., Chayes, D., Ferrini, V. & Wigley, R., 2015. A new digital bathymetric model of the world's oceans. *Earth and Space Science*.
<https://doi.org/10.1002/2015EA000107>

8.2 Data sources

Calder, B., Eriksson, B., Jerram, K., Weidner, E., Holmes, F., Muchowski, J., Prakash, A., Handl, T., Ståhl, E., Mayer, [...] 2020. High-resolution bathymetry from the Ryder 2019 expedition to Northwest Greenland. Dataset v1. Bolin Centre Database. <https://doi.org/10.17043/oden-ryder-2019-bathymetry-1> [accessed 2024-12-10]

ESA Greenland Ice Sheet CCI project team, 2018. Greenland Ice Velocity Map, Winter 2015-2016, v1.2. Centre for Environmental Data Analysis. <https://catalogue.ceda.ac.uk/uuid/302f379334e84664bd3409d08eca6565/> [accessed 2025-01-24]

Jakobsson, I., 2018. Kongsberg EM122 (1x1°) – Multibeam sonar. <https://www.su.se/geo/english-old/resources/list-of-all-equipment/list-of-field-equipment/kongsberg-em122-1x1-multibeam-sonar-1.380861> [accessed 2025-01-14]

Jakobsson, M., Mayer, L.A., Bringensparr, C., Castro, C.F., Mohammad, R., Johnson, P., Ketter, T., Accettella, D., Amblas, D., An, L., [...] 2020c. The International Bathymetric Chart of the Arctic Ocean Version 4.0. Scientific Data, 7(176).

Jakobsson, M., Mayer, L., Hogan, K., Eriksson, B., Jerram, K. & Stranne, C., 2021. High-resolution bathymetry from expedition Petermann, Northwest Greenland, 2015. Dataset v2. Bolin Centre Database. <https://doi.org/10.17043/oden-petermann-2015-bathymetry-2> [accessed 2024-12-10]

Jakobsson, M., Mohammad, R., Karlsson, M., Salas-Romero, S., Vacek, F., Heinze, F., Bringensparr, C., Castro, C.F., Johnson, P., Kinney, J., [...] 2024. The International Bathymetric Chart of the Arctic Ocean Version 5.0. Scientific Data 11(1420). <https://doi.org/10.1038/s41597-024-04278-w>

Appendix A

Within this appendix, the additional figures of a geological map displaying the bedrock types (Figure A1), a simplified version of the fjord terrain profiles (Figure A2) without the profile lines' positions, and a table describing the different submarine landforms (Table

A1) can be found. The legend to the geological map below can be retrieved from the GEUS (Geological Survey of Denmark & Greenland) website. Its main purpose within this study is to demonstrate the similarities of bedrock types around the three fjords.

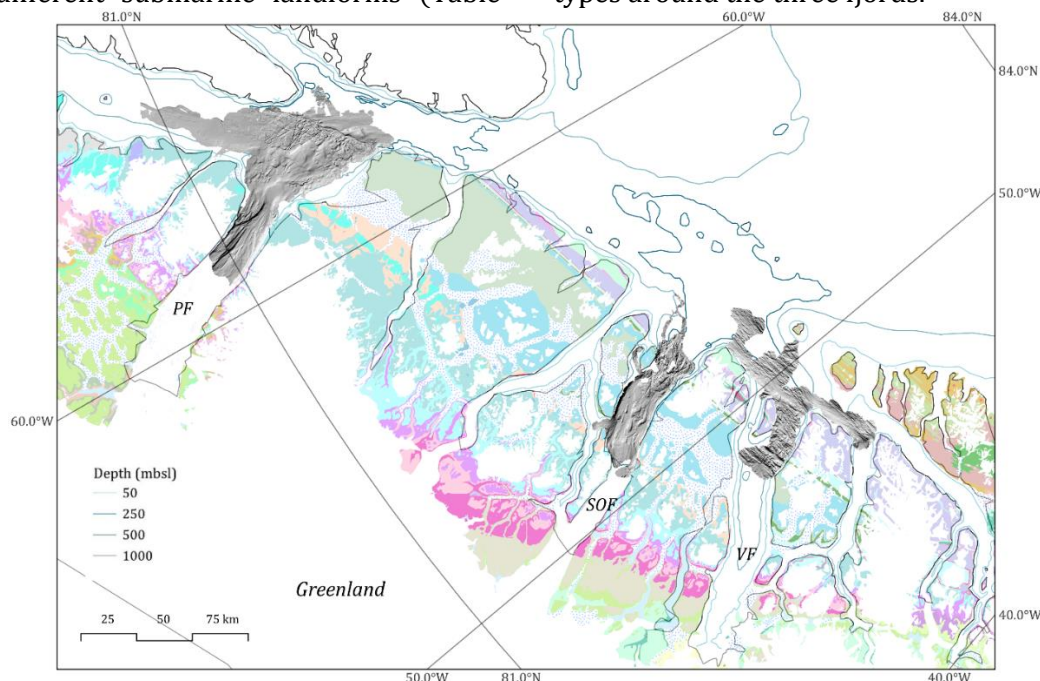


FIGURE A1 Geological map of the northern Greenland land surrounding the three fjords. The geological data is from Kokfelt et al. (2023), part of the Geological Survey of Denmark & Greenland (GEUS). Due to its extent the legend was omitted from this map. It can however be retrieved from the GEUS website.

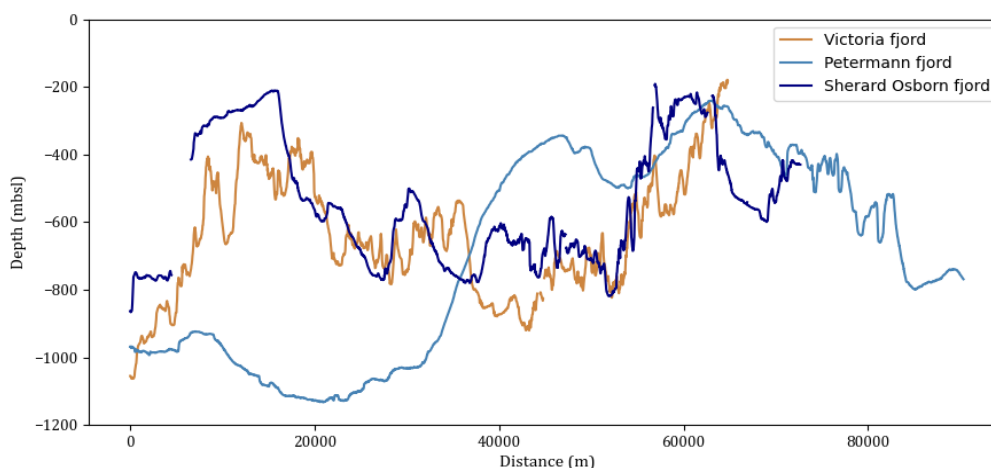


Figure A2 Diagram displaying the three terrain profiles drawn from the bathymetric data of the respective fjords. The Victoria fjord is displayed in a tan color, the Petermann fjord in a light blue, and the Sherard Osborn fjord in a darker blue. The x-axis shows distance from the start of the dataset, and the y-axis shows depth in mbsl, with negative numbers corresponding to sub-sea surface values.

TABLE A1 General descriptions of the identified glacial seafloor landforms and their respective roles in fjord studies. Rough bedrock, mentioned as a seafloor type throughout the paper, is omitted from this table as it is not a glacial landform.

Small-scale landform	General description	Role in fjords
<i>MSGLs</i>	Elongate parallel ridges in sediment aligned with ice flow direction.	Indicates fast or continuous ice flow, helping to reconstruct glacial history.
<i>Crag-and-tail</i>	Streamlined bedrock obstacles with sediment tail in the ice flow direction.	Gives clear indications of former ice flow direction.
<i>GZW</i>	Sedimentary deposit with a slightly rounded or oval shape.	Indicates standstill positions for the ice margin during retreat.
<i>Moraine</i>	Linear form perpendicular to the ice flow.	Shows past sites for ice margins.
<i>Iceberg ploughmark</i>	Randomly oriented and shaped lineations formed from scraping icebergs.	Hints at past iceberg calving activity.
<i>Meltwater channel</i>	Sinuuous wide deepenings of the seafloor where meltwater has flowed.	Helps in reconstructing past melting sites and water pathways.
<i>BS</i>	Large-scale ridge of bedrock or sedimentary origin, separating deeper basins.	Controls water inflow and temperatures within fjords.